VIDYASAGAR UNIVERSITY JOURNAL OF PHYSICAL SCIENCES

(A yearly publication of Vidyasagar University)

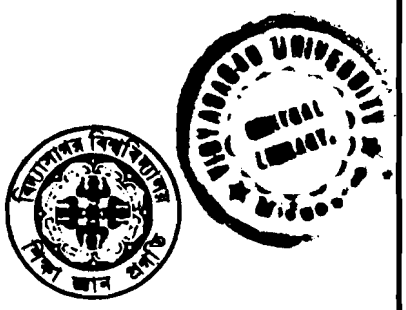

Volume 7 2001 - 2002

Vidyasagar University
Midnapore - 721 102
West Bengal
India

Editorial

Modern Information Technology Should lead us to the World of Social Justice.

Information Technology has been remarkably exploited in the applicational world of modern civilization since last two decades of our journey. Our future world will get it more and more in rational upgradation of its internal processes for formalisation of scientific, Social and cultural policies where information world is massively used with all its possible technological and spectacular features. Manipulations and distortions are also noticed in the analyses of several social and scientific cases where some sort of unwanted motivations are seen.

Therefore technologists should come forward immediately with their all technological back grounds so that the motivations can be removed. As like the circulation of blood in a healthy body, the distribution and circulation of proper informations to the society is deserved very much to get social justice in every aspect of regular life. In this context proper technology should also be developed with respect. Then with the help of the technology we can reach to a world of social justice.

Sourangshu Mukhopadhyay

Editor-in-Chief,
Vidyasagar University Journal of Physical Sciences

A THEORETICAL STUDY FOR FINDING PULSE BROADENING CHARACTER OF MULTIMODE GRADED INDEX FIBRE

Asmita Dasgupta,
Md Ahmadullah, Rupa Roy,
Panchanan Bhowmick,
Debkumar Chakraborty
and
Sourangshu Mukhopadhyay
Depertment of Physics and Technophysics
Vidyasagar University
Midnapur - 721 102, West Bengal, India.

Abstract :
A theoretical study for finding pulse broadening character of multimode graded index fibre is performed here with an alternative analysis.

INTRODUCTION

In contrast to an uniform refractive index core, in a graded refractive index fibre. refractive index in the core decreases continuously in a nearly parabolic character from a maximum value at the centre of the core to a constant value of at core-cladding interface. Due gradual decrease in the refractive index as one moves away from the centre of the core, a ray that enters the fibre in continuously bent towards the axis of the fibre. This follows from snell's law since as the ray proceeds away from the axis, it continuously encounters a medium of lower refractive index and hence bends away from its normal i.e. it bends towards the axis of the fibre. Such a graded index fibre reduces the transit time of rays, travelling obliquely by providing a larger velocity (due to lower refractive index) which partially compensates the relatively large optical path length that the ray has to traverse. Dispersion due to differences in transit time delays of different rays in such a fibre can be shown to be extremely low of the order of .05 ns/Km. Which is almost 1000 times better than an equivalent step index fibre. Thus such case graded refractive index profiled

fibres provide an extremely large information carrying capacity. We have considered the light propagation inside the fibre as a multimode of rays bouncing back and forth at the core-cladding interface. Such fibre which permit a large number of guided optical ray paths are known as multimode fibres. However it can be shown that if the diameter of the fibre shrinks or if the referactive index difference between the core and the cladding decreases the number of possible paths for wave guidance reduces. We will discuss in greater detail the pulse broadening character of graded index fibre.

PULSE DISPERSION

In digital communication systems, information to be sent is first coded in the form of pulses and then these pulses of light are transmitted from the transmiter to the receiver where the information is decoded. The larger the number of pulses that can be sent per unit time and still be resolvable at the receiver end, the larger is the transmission capacity of the system.

A pulse of light sent into a fibre brodens in time as it propagates through the fibre. This phenomenon is known as pulse dispersion and it happens because of the different times taken by different rays to propagate through the fibre. For example, in the fibre (Shown in fig. 1) the rays making larger angles with the axis have to traverse a longer Optical path length and they take a longer time to reach the output end. Consequently, the pulse broadens as it propagates through the fibre. Where the output pulses are not resolvable, no information can be received. Thus the smaller the pulse dispersion, the greater will be the information carrying capacity of the system.

Referreing to Fig, 1 for a ray making an angle θ with the axis, the distance AB in traversed in time $t = \dfrac{AC + BC}{c/n_1}$

$$= \frac{n_1(AB)}{c\cos\theta}$$

when c/n_1 represents the speed of light in a medium of refractive index n_1 with c as speed of light in free space, the time taken by a ray to traverse a length of the fibre will be

$t = n_1 L/C \cos\theta$.....(1)

Here L is the length of the fibre.

The abore expression shows that the time taken by a ray is a function of the angle θ made by the ray with the Z axis. If we assume that all rays between O and θc are present then the time taken by rays corresponding respectively between will be and by

$$t_{min} = n_1 L/C$$

$$t_{max} = \frac{L n_1^2}{C n_2}$$

Hence if all input rays were excited simultaneously, the rays will occupy a time interval at the out put end of duration $\Delta t = t_{max} - t_{min} = n_1 L/C(n_1/n_2 - 1)$

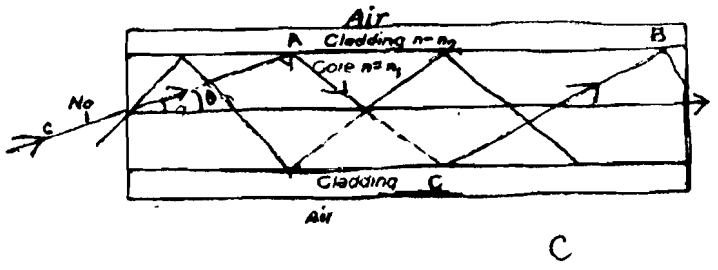

Fig. 1

For a typical fibre, if we assume
$n_1 = 1.46$, $\frac{n_1 - n_2}{n_1} = .01$, L = 1Km.

$\Delta t \approx 50 \times 10^{-9}$ s/Km = 50ns/Km.

i.e. an impulse after traversing through a fibre of length 1 Km broadens to a pulse of duration of about 50ns. Thus two pulses separated by say 500ns at the input end would be quite resolvable at the output end of 1 Km of the fibre however, if consecutive pulses are separated by, say 10ns at the input end, they would be absolutely unresolvable at the output-end. Hence in 1M bit/s fibre Optic system where we have one pulse in every 10^{-6} S; 50ns/Km. dispersion fibre system would require repeaters to be placed every 3 - 4 Km. On the other hand in 1000 M Bit/s fibre Optic communication system where we require the transmission of one pulse in every 10^{-9} S, a dispersion of 50ns/Km would result in intoberable broadening even within 50m which would be highly inefficient and uneconomical from a system point of view.

From the above discussion it follows that for a very high information carrying system, it is necessary to reduce the pulse dispersion, and thus two alternative solutions exit.One involving the use of graded index fibre and the other involving single mode fibre.

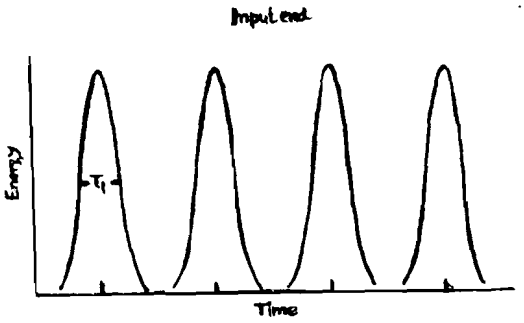

Fig. 2(a)

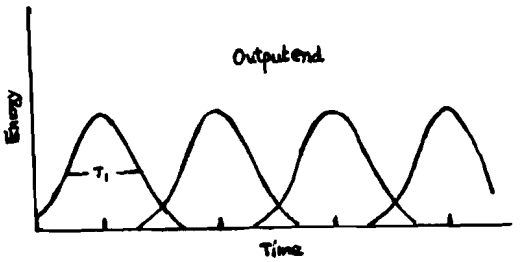

Fig. 2(b)

In fig. 2a series of pulses each of time width (at the input end of the fibre) τ_i after transmission through the fibre emerges as a series of pulses of width. If the broadening of the pulses is large, then adjacent pulses will overlap at the out put end and may not be resolvable. Out put is shown in fig. 2b.

Thus pulse broadening determines the maximum information carrying capacity of the optical fibre.

The dispersion mechanism involved in the pulse broadening comprises material dispersion, wave guide dispersion, intermodal dispersion. Inter modal dispersion may occur in all types of Optical fibre and results from finite spectral line width of optical source. Since, Optical sources could not emit single frequency but a band of frequencies (LED) then there may be propagation delay difference between the different spectral component of the transmittance signal. This cause broadening of each transmitted mode and hence intermodal dispersion. The delay difference may be caused by the dispersive properties of the wave guide material (i.e. called material clispersion) and also by guidance effect within the fibre structure i.e. wave guide dispersion.

We have considered the broadening of the Optical pulse by the fact that the different rays excited at the input end of the fibre take different times to propagate through the fibre. In addition, we have also material dispersion which is due to the fact that any light source has certain spectral width and different wavelength component travel with different group velocity. The broadening of a particular mode due to the finite spectral width of the source is known as intermodal dispersion. For highly multimoded step index fibres the intermodal dispersion is large and intermodal dispersion can be neglected. However, for multimode graded index fibres with nearly prabolic refractive index variation the intermodal dispersion is small and intermodal dispersion becomes important. Finally in single mode fibres, the dispersion has only the intermodal component.

In order to increase the information carrying capacity it is necessary to reduce material dispersion.

Typical characteristics of some fibre Optic.

Communication systems at different stages are given.

	Year	Bit rate	Type of fibre	Loss	Repeater Spacing (Km)
I. Generation (0.8 - 0.9 μm)	1977	~ 45 Mbit/S	Multi Mode (graded index)	~ 3	~10
II. Generation (1.3 μm)	1981	~ 45 Mbit/S	Multi Mode (graded index)	~ 3	~30
III. Generation (1.3 μm)	At present	~ 500 Mbit/S upgradables to ~ 1 Gb/S	Single mode	≤ 1	~40
IV. Generation (1.55 μm)	Immediate future	≥ 10g bits/S ≡ 15000 telephone channels	Single mode	< 3	≥ 100

Futuristic System : Infrared fibres ($\lambda_0 > 2$ μm)
Extremely low loss ($< 10^{-2}$ db/Km)
Repeater spacing > 1000 Km.

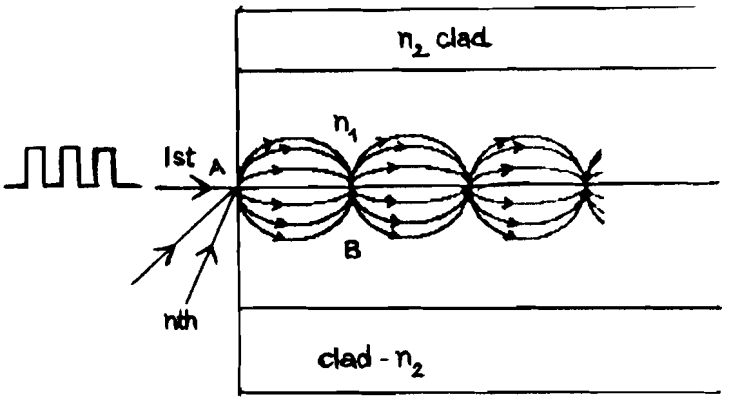

Fig. 3

We know the scalar wave equation of homogeneous the medium.

$$\nabla^2\psi = \epsilon_0\mu_0 n^2 \frac{\partial^2\psi}{\partial t^2} \quad \text{.....(1)}$$

In this section we will solve the scalar wave equation (1) for a parabolic index medium characterised by the following refractive index distribution $n^2 = n_1^2[(1 - 2\Delta/(\frac{r^2}{a^2})]$

$$= n_1^2[1 - \frac{2\Delta}{a^2}(x^2 + y^2)] \text{.....(2)}$$

where $\Delta = \frac{n_1 - n_2}{n_1}$ [$\because n_1 \neq n_2$]

a = Core redius

n_1 represent the axial refractive index. A medium characterised by equation (2) is usually referred to as an infinitily extended square law medium

We should mention again here that the refractive index variation given by eqn (2) can not be extended to infinity and in an actual fibre there is a boundary at r = a beyond which the refractive index is constant. However, the scaler wave equation can be solved exactly for an infinitely extended square law medium.

Such solutions gives a deep physical insight and also bring out most salient aspects of optical wave lengths.

if we substitude eqn (2) in the scalar wave equation we obtain.

$$\nabla^2\psi = \frac{n_1^2}{c^2}[1 - 2\Delta(\frac{x^2}{a^2} + \frac{y^2}{a^2})]\frac{\partial^2\psi}{\partial t^2} \quad \text{.....(3)}$$

We assume a solution of the form

$$\psi(x, y, z, t) = \psi(x, y)\, e^{i(\omega t - \beta z)} \quad \text{.....(4)}$$

Then equation (3) becomes

$$\frac{\partial^2\psi}{\partial x^2} + \frac{\partial^2\psi}{\partial y^2} + \{k_0^2 n_1^2[1 - 2\Delta\,(\frac{x^2}{a^2} + \frac{y^2}{a^2})] - \beta^2\}\,\psi = 0 \quad \text{.....(5)}$$

We use the method of separation of variables and write $\psi(x, y) = X(x)\, Y(y)$ ..... (6)

If we substitute the above solution in eqn (5) and divide by X(x) Y(y) we obtain

$$\left(\frac{1}{X}\frac{d^2X}{dx^2} - k_0^2 n_1^2 \frac{2\Delta}{a^2} x^2\right) + \left(\frac{1}{Y}\frac{d^2Y}{dY^2} - k_0^2 n_1^2 \frac{2\Delta}{a^2} y^2\right) + (k_0^2 n_1^2 - \beta^2) = 0 \quad \text{.....(7)}$$

The variables have indeed separated out and we may write

$$\frac{1}{X}\frac{d^2X}{dx^2} - k_0^2 n_1^2 \frac{2\Delta}{a^2} x^2 = \gamma_1 \quad \text{.....(8)}$$

$$\frac{1}{Y}\frac{d^2Y}{dY^2} - k_0^2 n_1^2 \frac{2\Delta}{a^2} y^2 = \gamma_2 \quad \text{.....(9)}$$

with $\beta^2 = k_0^2 n_1^2 - \gamma_1 - \gamma_2$ .....(10)

We now use the new variables such that

$$\left.\begin{aligned} \xi &= \alpha x \\ \eta &= \alpha y \end{aligned}\right\} \quad \text{.....(11)}$$

with $\alpha = \left(\frac{k_0^2 n_1^2 2\Delta}{a^2}\right) V = \frac{V^{1/2}}{a}$ .....(12)

Where $V = k_0 n_1 a (2\Delta)^{1/2}$ .....(13)

represents the wave guide parameters

Thus $\frac{d^2X}{d\xi^2} + (\lambda_1 - \xi) X(\xi) = 0$ ..... (14)

$$\frac{d^2Y}{d\eta^2} + (\lambda_2 - \eta) Y(\eta) = 0 \quad \text{.....} \quad (15)$$

where $\lambda_1 = \frac{\gamma_1}{\alpha^2} = \gamma_1 \left[\frac{a}{k_0 n_1 (2\Delta)^{1/2}}\right]$ ..... (16)

and $\lambda_2 = \frac{\gamma_2}{\alpha^2} = \gamma_2 \left[\frac{a}{k_0 n_1 (2\Delta)^{1/2}}\right]$ ..... (17)

For bounded solution i.e. for $X(\xi)$ and $Y(\eta)$

to tend to Zero as $\xi, \eta \rightarrow \pm \alpha$

must have $\lambda_1 = (2m + 1), m = 0, 1, 2$ ..... (18)

with $X(\xi) = X_m(\xi) = N_m H_m(\xi) e^{-1/2 \xi^2}$ .....(19)

where $H_m(\xi)$ are Hermite polynomials

$H_0(\xi) = 1, H_1(\xi) = 2\xi, H_2(\xi) = 4\xi^2 - 2$ ..... (20)
and N_m are the normalisation constant and given

by $N_m = \alpha^{1/2} / (2^n n! \pi^{1/2})^{1/2}$ ..... (21)

Such that $\int_{-\alpha}^{\alpha} X_m(x) X_{m'}(x) dx = \delta_{mm'}$ ..... (22)

Similarly for $\lambda_2 = \frac{\gamma_2}{\alpha^2} = \gamma_2 [\frac{a}{k_0 n_1 (2\Delta)^{1/2}}]$ ..... (23)

Where $\lambda_2 = 2n + 1, n = 0, 1, 2$ .....

and $Y(\eta) = N_n H_n(\eta) e^{-1/2 \eta^2}$ ..... (24)

$H_0(\eta) = 1, H_1(\eta) = 2\eta, H_2(\eta) = 4\eta^2 - 2$ ..... (25)

and the normalization constant N_n which is given
as $N_n = \alpha^{1/2} / (2^m m! \pi^{1/2})^{1/2}$ ..... (26)

$\beta^2 = k_0^2 n_1^2 - \gamma_1 - \gamma_2$ ..... (27)

where $\gamma_1 = \dfrac{\lambda_1}{[\dfrac{a}{k_0 n_1 (2\Delta)^{1/2}}]}$

and $\gamma_2 = \dfrac{\lambda_2}{[\dfrac{a}{k_0 n_1 (2\Delta)^{1/2}}]}$

$$\therefore \beta^2_{mn} = k_0^2 n_1^2 - \gamma_1 - \gamma_2$$

$$= k_0^2 n_1^2 - \frac{1}{\left[\frac{a}{k_0 n_1 (2\Delta)^{1/2}}\right]} [2m + 1 + 2n + 1]$$

$$= \frac{k_0^2 n_1^2 - 2k_0 n_1 (2\Delta)^{1/2} (m + n + 1)}{a}$$

$$= k_0^2 n_1^2 \left[1 - \frac{2(m + n + 1)(2\Delta)^{1/2}}{ak_0 n_1}\right]$$

$$\therefore \beta^2_{m,n} = k_0 n_1 \left[1 - \frac{2(m + n + 1)(2\Delta)^{1/2}}{ak_0 n_1}\right]^{1/2} \quad \text{..... (28)}$$

Thus for $m + n \angle\angle 10^3$, one is justified in making a binomial expansion in above eqn and if we retain only the ist order term we obtain

$$\beta_{m,n} \approx \left(\frac{\omega}{c_1}\right) n_1 - (m + n + 1) \left(\frac{2\Delta}{a}\right)^{1/2} \quad \text{..... (29)}$$

If we neglect the wavelength dependence of n_1 and Δ i.e. if we neglect material dispersion we get the very important result

$$\frac{d\beta_{m,n}}{d\omega} \approx \frac{n_1}{c} \text{ independent of m, n} \quad \text{..... (30)}$$

We know the group velocity of a particular mode is given by $v_g = \left(\frac{d\beta}{d\omega}\right)^{-1}$ ..... (31)

and therefore eqn (30) implies that different modes in a parabolic index fibre travel with almost the same group velocity. In the language of ray optics this approximately the same amount of time to propagate through the fibre. Therefore we can say

$$\boxed{t_n \approx t_0}$$

Now $\beta_{m,n} = k_0 n_1 \left[1 - \frac{2(m + n + 1)(2\Delta)^{1/2}}{ak_0 n_1}\right]^{1/2}$

Expanding the L.H.S. and we get

$$\beta_{m,n} = k_0 n_1 [1 - \frac{1}{2} \frac{2(m+n+1)(2\Delta)^{1/2}}{ak_0 n_1} - \frac{1}{8} \{ \frac{2(m+n+1)(2\Delta)^{1/2}}{ak_0 n_1} \} + \ldots\ldots\ldots]$$

$$= k_0 n_1 [1 - \frac{2(m+n+1)(2\Delta)^{1/2}}{ak_0 n_1} - \frac{2(m+n+1)^2(\Delta)}{a^2 k_0^2 n_1^2}]$$

$$= k_0 n_1 - \frac{(m+n+1)(2\Delta)^{1/2}}{a} - \frac{(m+n+1)^2(\Delta)c}{a^2 \omega n_1} \quad [k_0 = \omega/c]$$

$$\therefore \beta_{m,n} = (\frac{n_1}{c}) \omega - \frac{(m+n+1)(2\Delta)^{1/2}}{a} - \frac{c(m+n+1)^2(\Delta)}{a^2 n_1} \frac{1}{\omega} \quad \ldots\ldots\ldots\ldots (32)$$

$$\frac{d\beta_{m,n}}{d\omega} = \frac{n_1}{c} - 0 + \frac{c(m+n+1)^2(\Delta)}{a^2 n_1} \cdot \frac{1}{\omega^2}$$

$$= \frac{n_1}{c} + \frac{c(m+n+1)^2}{a^2 n_1} (\frac{n_1 - n_2}{n_1}) \cdot \frac{1}{\omega^2}$$

$$= \frac{n_1}{c} + \frac{\Delta . c(m+n+1)^2}{a^2 n_1} \cdot \frac{1}{\omega^2}$$

$$\therefore \frac{d\beta_{m,n}}{d\omega} = \frac{n_1}{c} + \frac{\Delta c(m+n+1)^2}{a^2 n_1} \cdot \frac{1}{\omega^2} \quad \ldots\ldots\ldots\ldots (33)$$

$$\therefore v_g = [\frac{n_1}{c} + \frac{\Delta c}{a^2 n_1} (m+n+1)^2 . \frac{1}{\omega^2}]^{-1} \quad \ldots\ldots\ldots\ldots (34)$$

$$v_g = (\frac{n_1}{c} + \frac{\Delta c(m+n+1)^2}{a^2 n_1} . \frac{1}{\omega^2})^{-1}$$

If the length of the fibre will be L then we have the different value m, n and we can find out the time to travel in the fibre. We have considered some cases

(I) $m = 0,\ n = 0$

$$v_{g_I} = \left(\frac{n_1}{c} + \frac{\Delta c}{a^2 n_1}\cdot\frac{1}{\omega^2}\right)^{-1}$$

$$\therefore t_I = \frac{1}{v_{g_I}} = L\left(\frac{n_1}{c} + \frac{\Delta c}{a^2 n_1 \omega^2}\right)$$

(II) $m = 1,\ n = 1$

$$v_{g_{II}} = \left[\frac{n_1}{c} + \frac{9\Delta c}{a^2 n_1 \omega^2}\right]^{-1}$$

$$\therefore t_{II} = \frac{1}{v_{g_{II}}} = L\left[\frac{n_1}{c} + \frac{9\Delta c}{a^2 n_1 \omega^2}\right]$$

(III) $m = 0,\ n = 1$

$$v_{g_{III}} = \left[\frac{n_1}{c} + \frac{4\Delta c}{a^2 n_1 \omega^2}\right]^{-1}$$

$$\therefore t_{III} = \frac{L}{v_{g_{III}}} = L\left[\frac{n_1}{c} + \frac{4\Delta c}{a^2 n_1 \omega^2}\right]$$

(IV) $m = 1,\ n = 0$

$$v_{g_{IV}} = \left[\frac{n_1}{c} + \frac{4\Delta c}{a^2 n_1 \omega^2}\right]^{-1}$$

$$\therefore t_{IV} = \frac{L}{v_{g_{IV}}} = L\left[\frac{n_1}{c} + \frac{4\Delta c}{a^2 n_1 \omega^2}\right]$$

If we ensume that

$\Delta = .01$

$n_1 = 1.46$

$a = 25 \times 10^{-6}$ m

L = 1km
$w = 2.4 \times 10^{15}$ Hz
Then for Case - I, where m = 0, n = 0

$$t_I = 1000 \left[\frac{1.46}{3 \times 10^8} + \frac{.01 \times 3 \times 10^8}{(25 \times 10^{-6})^2 \times (1.46) \times (2.4 \times 10^{15})^2} \right]$$

$$= 10^3 [.487 \times 10^{-8} + .5707 \times 10^{-15}] \text{ sec}$$

Case - II
Similarly, for m = 1, n = 1

$$t_{II} = 1000 \left[\frac{1.46}{3 \times 10^8} + \frac{9 \times .01 \times 3 \times 10^8}{(25 \times 10^{-6})^2 \times 1.46 \times (2.4 \times 10^{15})^2} \right]$$

$$= 10^3 [.487 \times 10^{-8} + 5.137 \times 10^{-15}] \text{ sec}$$

So $t_{II} - t_I = (5.137 - .5707) \times 10^{-12}$ sec
$= 4.5663 \times 10^{-12}$ sec

Now for Case - III
m = 0, n = 1

$$t_{III} = 10^3 \left[\frac{1.46}{3 \times 10^8} + \frac{4 \times .01 \times 3 \times 10^8}{(25 \times 10^{-6})^2 \times 1.46 \times (2.4 \times 10^{15})^2} \right]$$

$$= 10^3 [.487 \times 10^{-8} + 2.2831 \times 10^{-15}] \text{ sec}$$

$t_{III} - t_I = 10^3 (2.2831 - .5707) \times 10^{-15}$ sec
$= 1.7123 \times 10^{-12}$ sec
$t_{III} - t_{II} = 10^3 (5.137 - 2.283) \times 10^{-15}$ sec
$= 2.854 \times 10^{-12}$ sec

Again if we choose different modes
For Case I L = 10km, m = 10, n = 10
i.e. $L = 10^4$m

$t_0 = 10^4(.487 \times 10^{-8})$ sec

$$t_n = 10^4 \left[\frac{1.46}{3 \times 10^8} + \frac{(21)^2 \times .01 \times 3 \times 10^8}{(25 \times 10^{-6})^2 \times 1.46 \times (2.4 \times 10^{15})^2}\right] \text{ sec}$$

$= 10^4 [.487 \times 10^{-8} + 2.51 \times 10^{-15}]$ sec

$t_n - t_0 = 2.51 \times 10^{-9}$ sec

For Case - 2 L = 10km = 10^4m, m = 50, n = 50

$t_n = 10^4[.487 \times 10^{-8} + (101)^2 \times 5.7077 \times 10^{-16}]$ sec

$= 10^4[.487 \times 10^{-8} + 5.82 \times 10^{-12}]$ sec

$t_n - t_0 = 10^4 (5.82 \times 10^{-12})$ sec $= 5.82 \times 10^{-8}$ sec

Now for Case - 3 L = 10km, m = 100, n = 100

i.e. L = 10^4m

$$t_n = 10^4 \left[.487 \times 10^{-8} + \frac{(201)^2 \times .01 \times 3 \times 10^8}{(25 \times 10^{-6})^2 \times 1.46 \times (2.4 \times 10^{15})^2}\right] \text{ sec}$$

$= 10^4[.487 \times 10^{-8} + 2.3 \times 10^{-11}]$ sec

$t_n - t_0 = 2.3 \times 10^{-7}$ sec

Where as for Case - 4 L = 10km = 10^4m, m = 200, n = 200

$t_n = 10^4[.487 \times 10^{-8} + (401)^2 \times 5.7 \times 10^{-16}]$ sec

$= 10^4[.487 \times 10^{-8} + 9.16 \times 10^{-11}]$ sec

$\therefore t_n - t_0 = 9.16 \times 10^{-7}$ sec

And finally for Case - 5 t = 10^4m m = 250, n = 250

$t_n = 10^4[.487 \times 10^{-8} + (501)^2 \times 5.7 \times 10^{-16}]$ sec

$= 10^4[.487 \times 10^{-8} + 1.43 \times 10^{-10}]$ sec

$t_n - t_0 = 1.43 \times 10^{-6}$ sec

CONCLUSION

The time taken by axial ray to traverse a length L of the fibre $t_0 = \frac{L}{v_{g_1}} = L(v_{g_1})^{-1}$

$[v_g = (\frac{d\beta_{mn}}{d\omega})^{-1} = (\frac{n_1}{c} + \frac{\Delta c(m+n+1)^2}{a^2 n_1} \cdot \frac{1}{\omega^2})^{-1}]$

and the time taken by meriodional ray (nth) to traverse a length L of the fibre

$$t_n = \frac{L}{v_g} = L(\frac{d\beta_{mn}}{d\omega})^{-1} = L(\frac{n_1}{c} + \frac{\Delta c(m+n+1)^2}{a^2 n_1} \cdot \frac{1}{\omega^2})$$

For axial ray $t_0 = L\frac{n_1}{c}$

Putting the different values of m, n, & L we get dispersion. We obtain that dispersion due to the differences in transit time delays of different rays in such a fibre can be shown to be externely low. Then we conclude that time spent to cover the distance (L) between A and B in figure 3 for the ray marked by n (t_n) and that of the ray marked by 1 (to) is approximately same

$\therefore$ $\boxed{t_n \approx t_0}$

From calculation we get different time delays in the range of 10^{-6} sec to 10^{-9} sec by selecting different modes, so from these results we can choose different modes of light rays in a graded index fibre in the pulse frequency range of 10^6HZ to 10^9 HZ.

REFERENCES

[1] A. K. Ghatak and K. Thyagarajan, - 'Optical electronics' Cambridge University Press (1989).

[2] Arnaud, J. A. (1976), 'Beam and Fibre optics' Academic Press New York.

[3] Mid Winter, J (1979), 'Optical fibrel of Transmission' John Wiley New York.

[4] M. K. Barnoski(ed), 'Fundamentas of optical fibre Communication' Academic Press, New York, 1976, Section 2, 3, 1.

[5] R. Olshansky, 'Propagation in glass optical wave guides' Rev. Mod. Phys., 51(2), 1979, 341.

[6] J. E. Midwinter, OP. Cit., chapters 10,11.

THE EFFECT OF A TRANSVERSE MAGNETIC FIELD ON A SUBNORMAL REGION IN DISCHARGE IN HYDROGEN

D. C. Jana and S. S. Pradhan
Department of Physics and Technophysics
Vidyasagar University
Midnapur - 721 102, West Bengal, India.

Abstract :
The discharge in Subnormal region under d.c. excitation at different pressure in a varying transverse magnetic field (0 to 42 G) some measurements have been carried out for various initial average tube currents. The voltage across the discharge increases and average tube current, residual current decreases in the magnetic field. Using the Beckman's expression (1) for the axial field and the electron density distribution in a transverse magnetic field the observed variation of current and voltage can be satisfactorily explained. The variation of axial electric field with transverse magnetic field can be represented to a fair degree of accuracy by the derived equation. The reaction of residual current with magnetic field has been observed in these oscillations.

Key words : Subnormal region, residual current, electron density.

INTRODUCTION

In the previous paper (Jana and Pradhan [2]) the variation of average tube current and axial voltage across the tube and residual current for air in transverse magnetic field (0 to 30 G) were measured when the initial constant currents 100, 120 and 150 μA. It was found that the discharge current decreases with increase of the transverse magnetic field and the result can be analytically explained by the Beckman theory. The axial voltage increases in the presence of a magnetic field and the slope of the curve should give the value of $C_1(e/m. L/v_r)$. A quantitative explanation has been provided for the variation of the residual current with the transverse magnetic field. The purpose of the present investigation is to watch carefully the effect of the transverse magnetic field on a subnormal glow discharge in hydrogen, experimentally.

EXPERIMENTAL ARRANGEMENT

The method of measuring the effect of transverse magnetic field on hydrogen is the same as in the previous paper (Jana and Pradhan [2]). Spectroscopically pure hydrogen sample supplied by British Oxygen Co. Ltd. The gas has been collected in an evacuated chamber and passed through a needle valve. To start with the pressure has been kept fixed by a micro-leak needle valve at 0.5 Torr and the output voltage of the power supply adjusted so as to obtain average tube current in the circuit.

RESULTS AND DISCUSSIONS

The extent to which a thing changes of average tube current and the corresponding axial voltage accross the tube are plotted in the figure 1, 2 and 3 for initial tube current 150μA, 175μA and 200μA respectively at constant pressure 0.5 Torr as three representative cases. It is found that the current decreases gradually with the increase of the magnetic field and the voltage across the tube increases. The residual current has also been computed and the variation of I_{rH} (residual current against the magnetic field) has been observed and plotted in figure 4 for different values of initial current. It is noted that the residual current decreases with the increase of the magnetic field. A simple explanation of the noted results can be given. The glow is excited by a d.c. source of voltage E_{dc} in series with resistance R. In the absence of the magnetic field, the voltage drop across the subnormal region $V_0 = E_{dc} - IR$, where I is the initial current. Under the action of the transverse magnetic field, electrons are deviated from their straight line path and can not contribute to the main current, which decreases. In the future, if V_H is the voltage drop across the tube in the presence of the magnetic field, $V_H - V_0 = R(I - I_{rH})$ and as I_{rH} is less than I, so V_H will be greater than V_0.

The effect of a transverse magnetic field on the positive column of a glow discharge has been investigated by Beckman(1). He showed that the axial voltage increases in the presence of a magnetic field from E to

$$E(\alpha + \beta^2/\alpha)^{1/2},$$

where

$$\alpha = 1 - h^2 + h^4 \exp h^2 \int_h^0 \frac{\exp(-h)}{h}\, dh$$

$$\beta = \frac{h}{2}\sqrt{\pi}\,(1 - 2h^2 + 4h^3 \exp h^2 \int_h^\infty \exp(-h^2)dh),$$

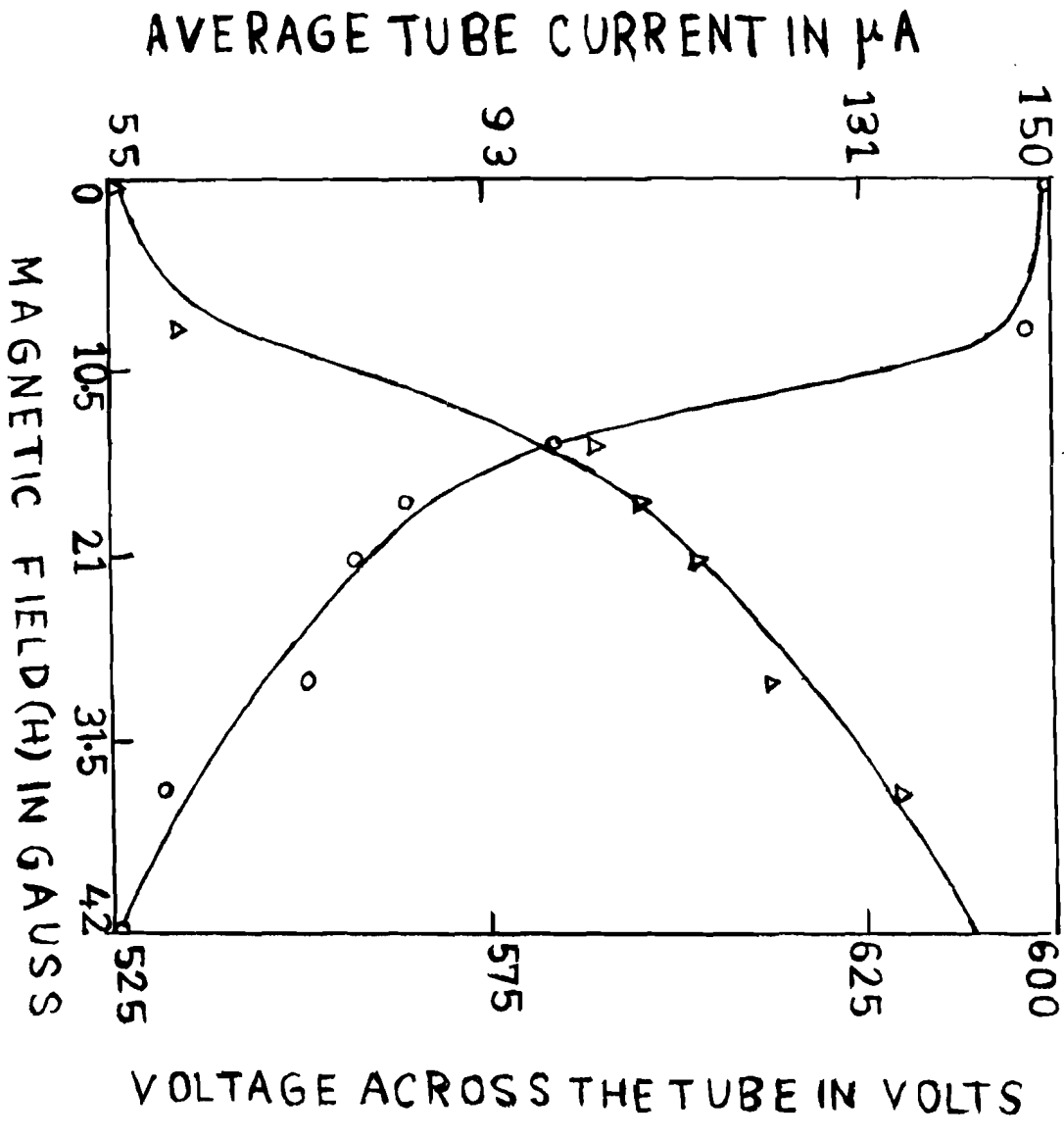

Figure - 1 : Variation of average tube current and axial voltage across the tube. Initial tube current 150 μA.

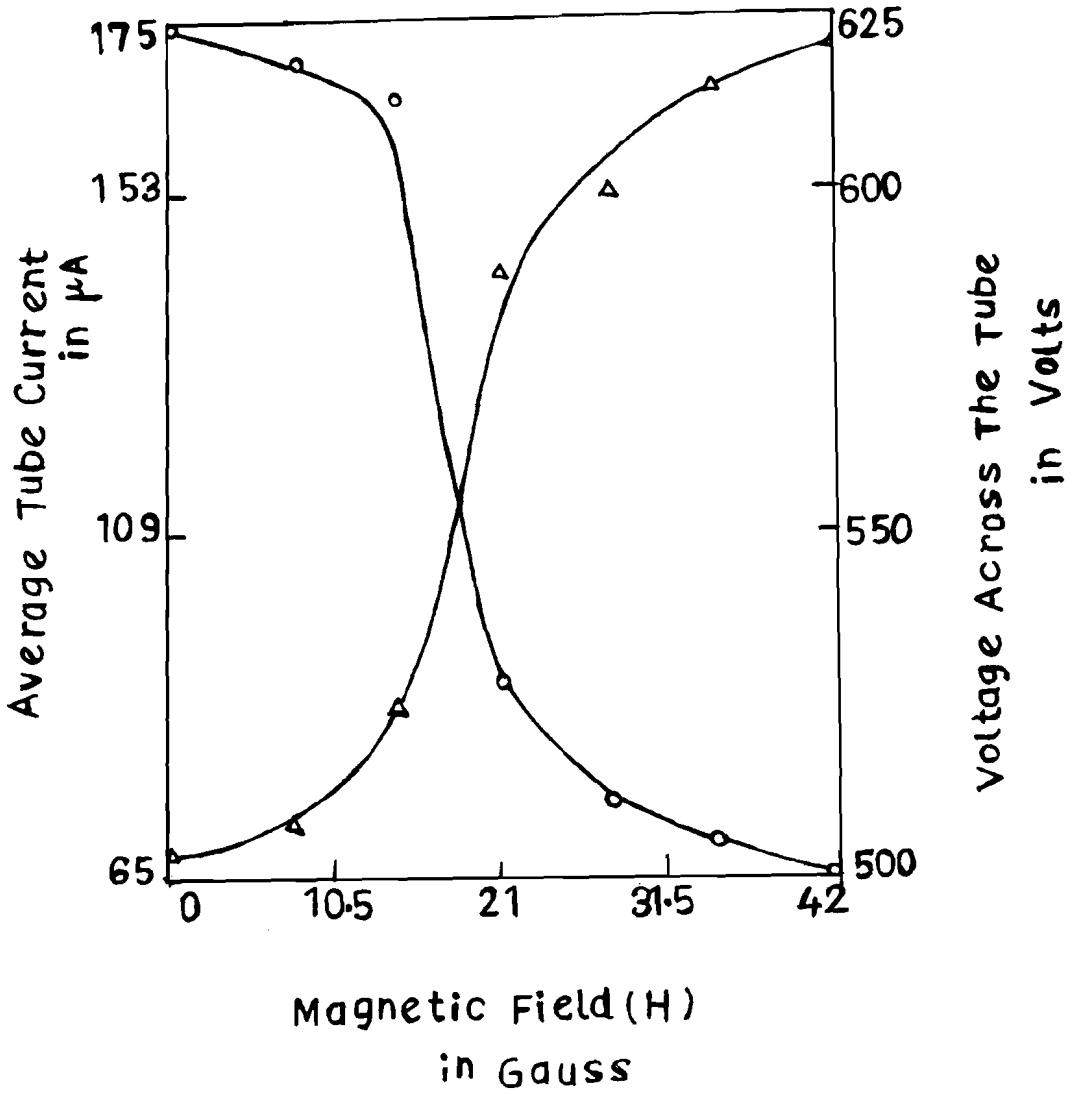

Figure - 2 : Variation of average tube current and axial voltage across the tube. Initial tube current 175 μA.

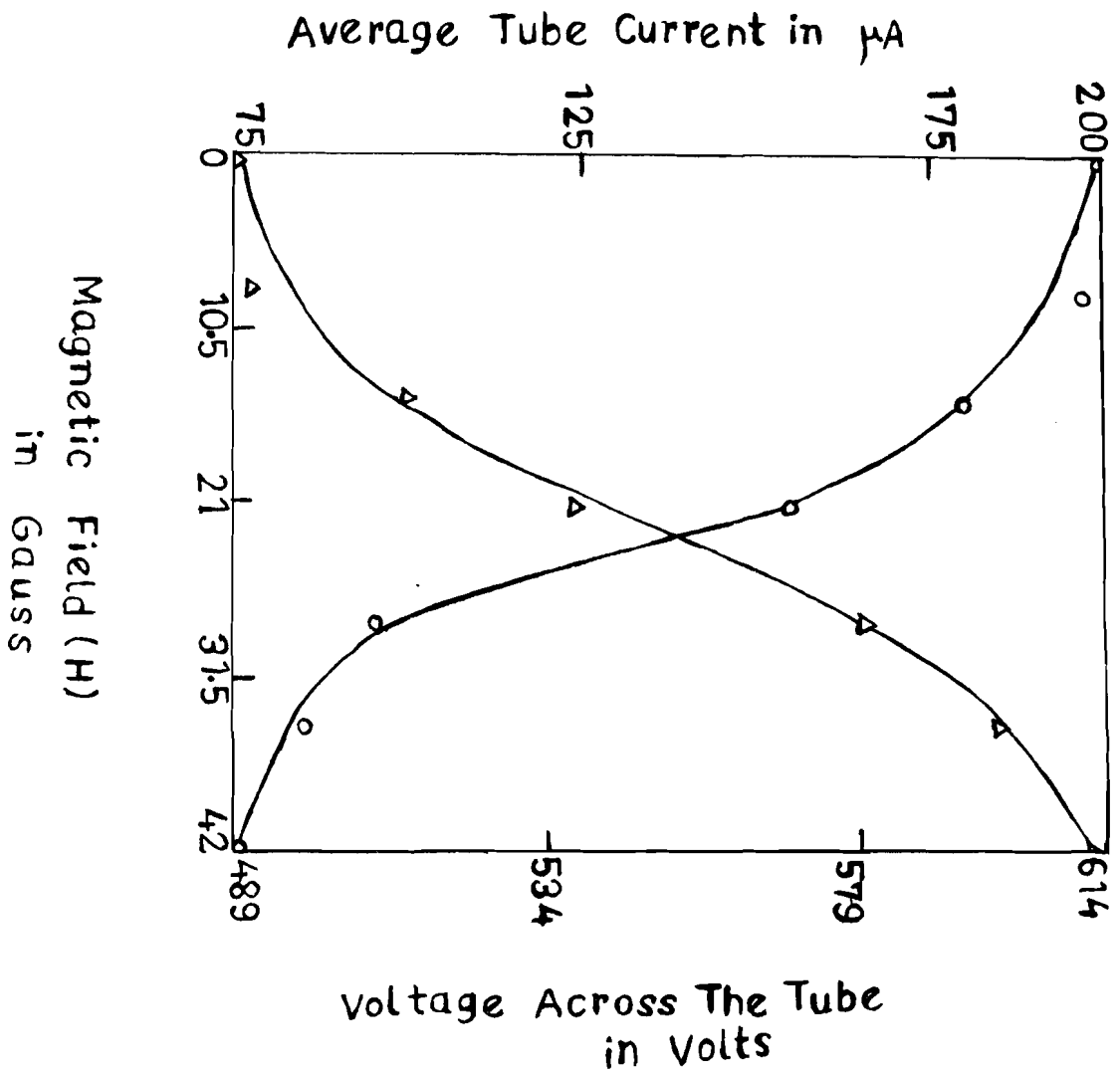

Figure - 3 : Variation of average tube current and axial voltage across the tube. Initial tube current 200 μA.

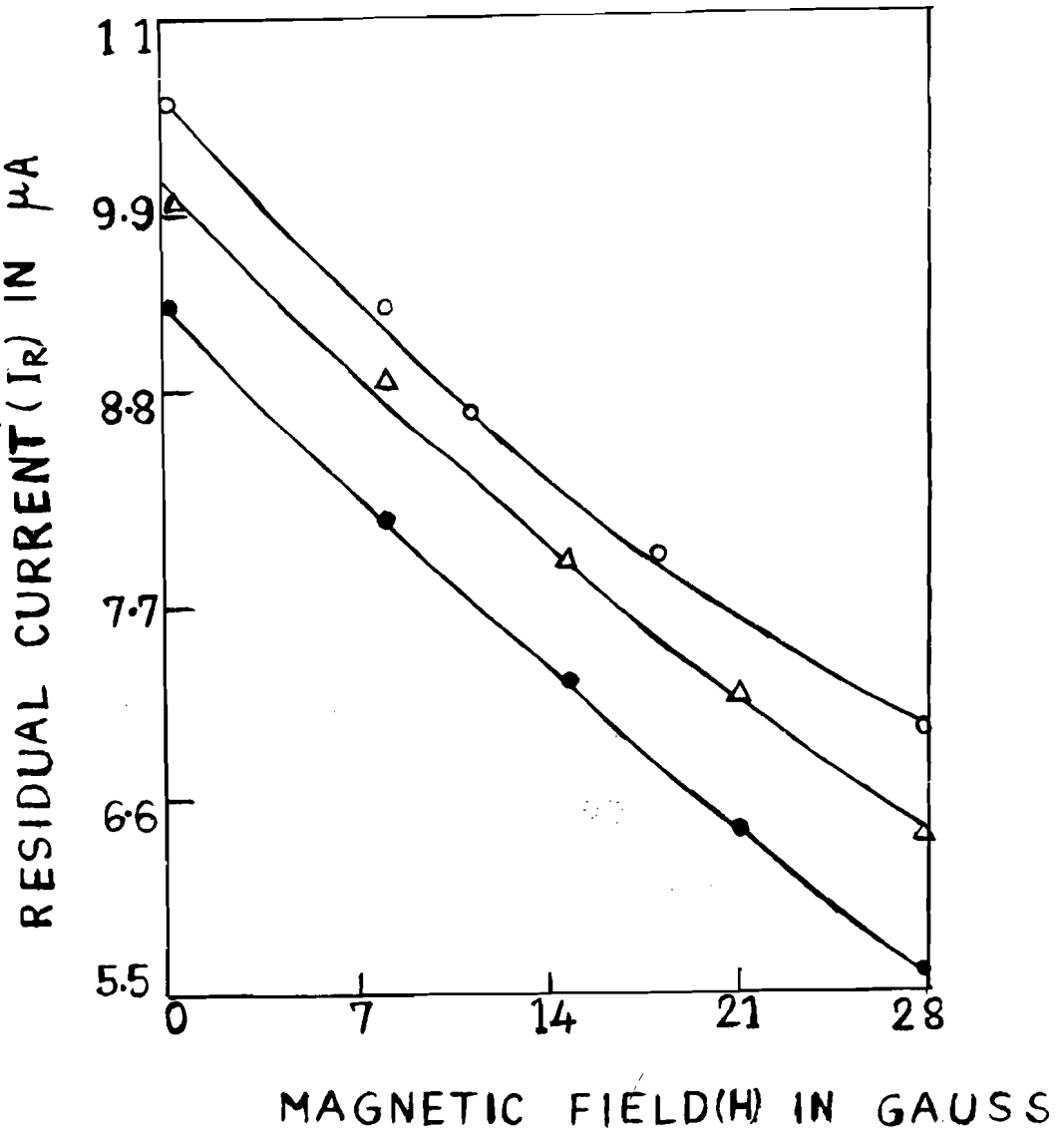

Figure - 4 : Variation of residual current with magnetic fields, Initial tube current [I] 150 μA. [II] 175 μA. [III] 200 μA.

$$h = \frac{2H\lambda}{m\omega}$$

where H is the magnetic field

λ is the m.f.p.

ω is the most probable electronic speed.

$\omega^2 = 2KT_e/m$ and $h = 2eHh/mpv_r \sqrt{H}$

L is the m.f.p. of the electron in the gas at a pressure of 1 Torr,

$Vr = (8KTe/m\pi)^{1/2}$,

As h is small for the values of magnetic field used in the experiment,

$\beta = h/2\sqrt{\pi} = eHL/mvrp$ and $\alpha = 1$.

Hence, $E_H = E(1 + C_1H^2/P^2)^{1/2}$,

Where C_1 is constant for a particular gas which is given by $C_1 = (e/m.\ L/v_r)^2$

Therefore, $(E_H^2 - E^2)/E^2 = C_1H^2/P^2$.

As the pressure is kept constant, the variation of $(E_H^2 - E^2)/E^2$ against H^2/P^2 or simply against H^2 should be straight line and the slope of the curve should give the value of C_1. The change has been plotted in figure 5 for all the three initial discharge currents and the curves are passing thruogh the origin which shows that the derived equation $E_H = E(1 + C_1 H^2/P^2)^{1/2}$ can be represented to a fair degree of accuracy the variation of axial electric field with transverse magnetic field. It is evident from figure 5, that the points lie approximately on the straight line upto H/P = 40 G/Torr and beyond this there is a gradual diversion from straight line behavior. The values of C_1 as calculated from the curves for different initial currents has been entered in table 1.

Additional, if Ir(residual current) is in the absence of the magnetic field then in the presence of the magnetic field residual current

$$Ir_H = \frac{\text{Shift due to magnetic field(cm) X Sensitivity (V/cm}^{-1})}{\text{resistance}}$$

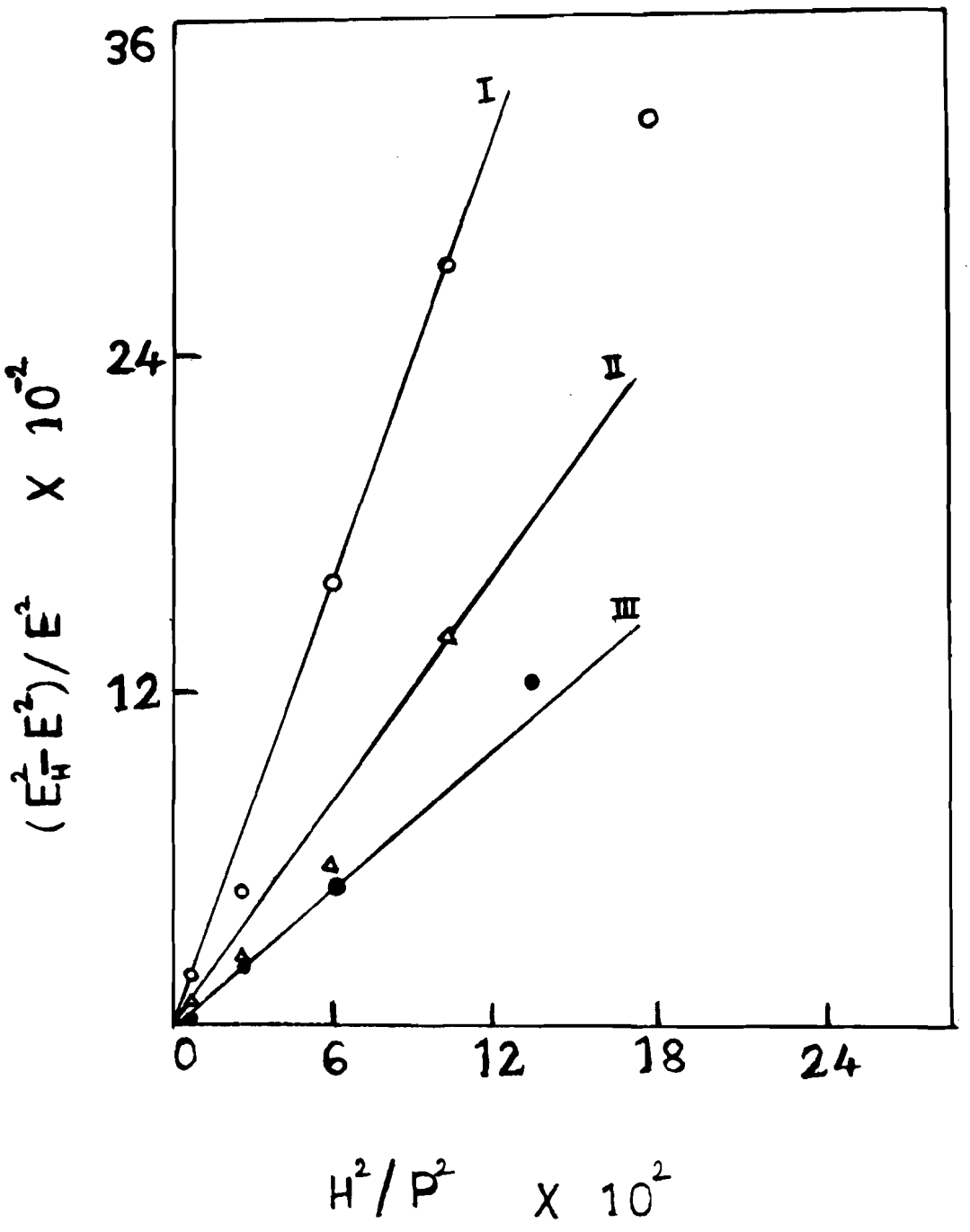

Figure - 5 : Variation of $(E_H^2 - E^2)/E^2$ against H^2 / P^2, Initial tube current [I] 150 μA. [II] 175 μA. [III] 200 μA.

will decrease.

The closeness of the residual current suggests that the discharge tube is not completely switched off between two successive pulses so far as the breakdown is concerned but a small amount of current always keep flowing through it. The loss ions and electrons between successive pulses can be attributed to processes such as ambipolar diffusion volume recombination and attachment [3]. In this existing experimental conditions, ambipolar diffusion is likely to dominate. In the present study with transverse magnetic field the loss of electrons is less prominent than that of ions because the diffusion of electron is less than that of ions and hence residual current with increasing transverse magnetic field decreases and also indicates the possibility of measuring the time needed for almost complete loss at ions and electrons during the passage of a pulse.

TABLE - 1

Initial current (μA)	C_1
150	$2.6 * 10^{-4}$
175	$1.4 * 10^{-4}$
200	$0.83 * 10^{-4}$

CONCLUSION

It can thus be conclude that the effect of transverse magnetic field on the subnormal region should follow the Beckman's theory also for molecular gases.

REFERENCES

[1] L.Beckman. Proc. Phys. Soc. 61,515 (1948)

[2] D.C. Jana and S. S. Pradhan, Pramana - journal of Physics Vol. 56, No. 1, January 2001, 107 - 115.

[3] G.Francies, Ionization Phenomena in gases [Butterworths Scientific Publication, London 1960].

MICROSTRUCTURAL CHARACTERIZATION OF THIN FILMS OF COPPER

S. Chandra, S. Dutta, N. K. Ghosh, T. K. Das, P. Mishra & S. Saha
Dept. of Physics & Technophysics
Vidyasagar University
Midnapur - 721 102, West Bengal, India

INTRODUCTION

Thin films of copper are grown on glass as well as on mica at various substrate temperatures using thermal vacuum evaporation technique. X-ray diffraction patterns of vacuum deposited thin films of copper have been recorded. Grain size as well as stacking fault probability of the films grown at various conditions have been estimated from X-ray diffraction profile. An attempt has been made to find suitable conditions to grow good quality films of copper on glass as well as on mica. Also XPS analysis has been carried to verify whether the films are free from oxide or not.

EXPERIMENTAL DETAILS

The films are deposited by evaporating specpure copper strip from a quartz crucible placed in a tungsten coil on properly cleaned glass and mica substrates. The deposition is done in a vacuum of the order of 10^{-6} torr using a Hind Hivac Vacuum Coating Unit (model 12 - A4). Films are grown at various substrate temperatures (35^0 C, 85^0 C and 125^0C). Simultaneously a glass and a mica substrate is placed on the substrate holder at each deposition condition. During each deposition the substrate to holder distance (4 inch), rate of deposition (3.5 nm s^{-1}), quantity of the materials (1 gm), vacuum condition (10^{-6} torr) are kept fixed. As a result the films deposited at various substrates temperatures on glass as well as on mica have nearly constant thickness. The thickness of the films are measured by Surfometer (SF 101). The thickness of various films are found to vary within the range of 7000 - 7250 A^0. X-ray diffraction data are recorded with a Philips x-ray diffractometer using monochromatic Cuk_α radiation. X-ray Photoelectron Spectroscopy has been carried on copper film using ESCA spectrometer.

RESULTS AND DISCUSSIONS

The diffraction profile for (111) peak of bulk copper and for films deposited on glass and mica at various substrate temperatures are shown in figure 1 and 2 respectively. X-ray diffraction pattern of bulk copper as well as copper films on different substrates show polycrystalline nature of the material. The average size of the crystallites are determined from the Scherrer formula (1-2).

$$P = K\lambda / \beta_{1/2} \cos\theta$$

P is the crystallite size,
λ is the wavelength of x-rays,
θ is the Bragg angle,
$\beta_{1/2}$ is the width of the peak at half maximum intensity

The stacking fault probability are estimated from the peak shift of the x-ray lines with reference to that from well annealed samples, using the method given by warren and warekois (3).

The formula used to calculate is given by

$$\alpha = \frac{(2\theta_F - 2\theta_B)}{45\sqrt{3}\ \tan\theta_F}$$

$2\theta_B$ is the angle corresponding to the (111) peak of the bulk.
$2\theta_F$ is the angle corresponding the (111) peak of the film

TABLE - 1

Substrate	Film Thickness (A^0)	Substrate Temperature (^0C)	Crystallite Size (A^0)	Stacking Fault Probability (α) 10^{-5}
GLASS	7220	35	139	84
	7190	85	281	7
	7050	125	308	132
MICA	7220	35	261	70
	7190	85	274	166
	7050	125	263	215

The crystallite size increases sharply as the film is deposited at higher substrate temperature (85°C) and becomes maximum at 125°C substrate temperature. Hence it is observed rate of increase of grain size is sharper initially and much slower at higher substrate temperature. This is possibly due to the fact that with increase in substrate temperature greater re-evaporation and diffusion in the disordered region leads to recrystallisation. The slower rate of increase of crystallite size at higher substrate temperature is due to the increase of stacking fault probability.

The crystallite size reaches close to maximum value for the film deposited on mica at room temperature. With increase of substrate temperature the size increases very slightly and decreases at the highest substrate temperature. The appearance of higher crystallite size on mica even at room temperature is due to the crystallite nature of mica. This is not in case of glass due to its amorphous nature. The larger increase of stacking fault probability for the films deposited on mica at higher substrate temperature is due to the faulting mechanism between the transition region of structure i.e. mica to copper.

XPS study has been done on the film to verify if there is any oxide formation on the film surface. XPS spectrum shows peaks for different electrons in copper (Core electrons, Valence electrons, Auger electrons). XPS spectrum (Fig. 3) indicates binding energy of these electrons and also specify different levels in which these electrons belong.

TABLE - 2

XPS of copper film	Binding energy (ev)	Level Identification
Core Electron	1097 953 933	$2S_{1/2}$ $2P_{1/2}$ $2P_{3/2}$
Valence electron	123	$3S_{1/2}$
Auger electron	568 648 769	$L_3M_{45}M_{45}$ $L_3M_{23}M_{45}$ $L_3M_1M_{23}$

Auger peaks are due to LMM transitions (initial hole in the L shell, transition of an M electron into the hole, followed by emission of another M electron).

Most important aspect of this investigation that no peak corresponding to copper oxide is found out. From figure - 4 (Drawn from Handbook of X-ray Photoelectron Spectroscopy) it is well known (4) that copper oxide peak appear as shake up satellite in between the peaks $2P_{1/2}$ & $2P_{3/2}$. But no such satellite is observed in our experimental result (Fig. 3). Hence it can be concluded that the film of copper are of good quality & free from any oxide.

REFERENCES

[1] Introduction to crystal and lattice defects, By S. Bhattacharjee & G. D. Nigam, page 167.

[2] A. J. C. Wilson, Proc. Phys. Soc., 80 (1962) 286.

[3] B. E. Warren and E. P. Warekois, Acta Metall, 3 (1955) 473.

[4] Handbook of X-ray photoelectron Spectroscopy, Perkin-Elmer, Page 83.

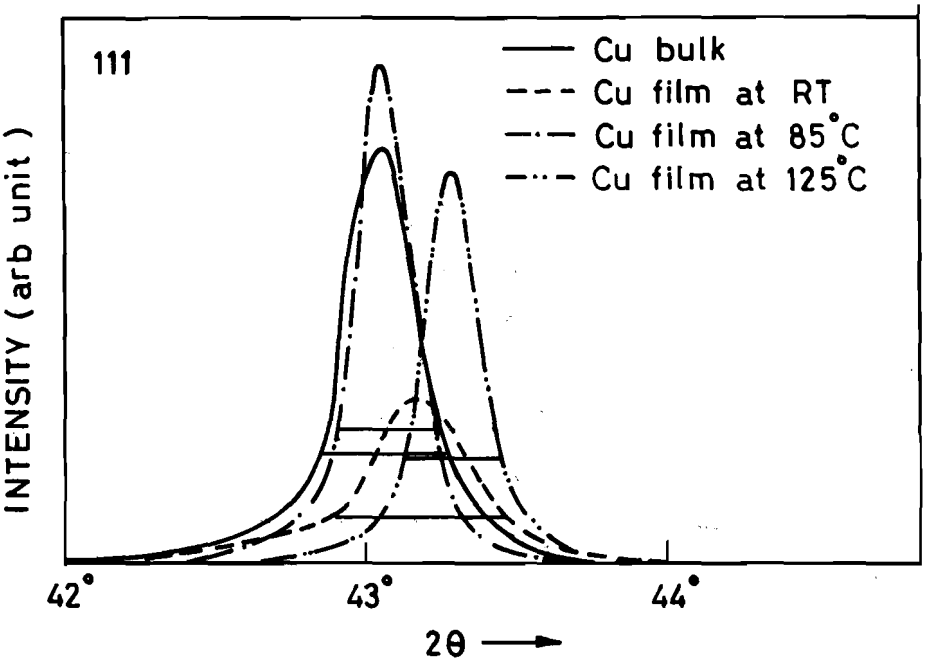

Fig. 1 Peaks of copper bulk and films deposited on glass at various substrate temperatures

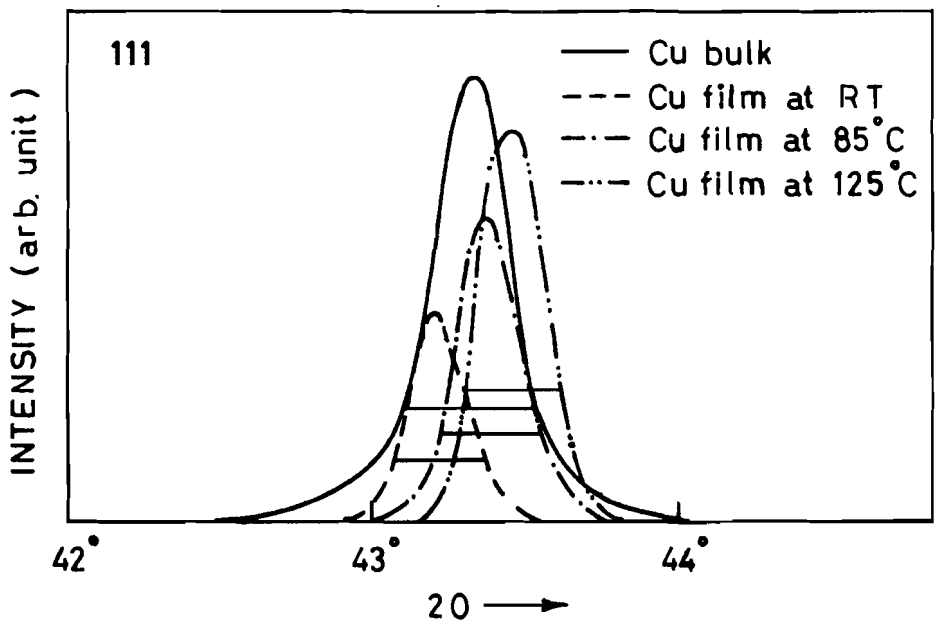

Fig. 2 Peaks of copper bulk and copper films deposited on mica at various substrate temperatures

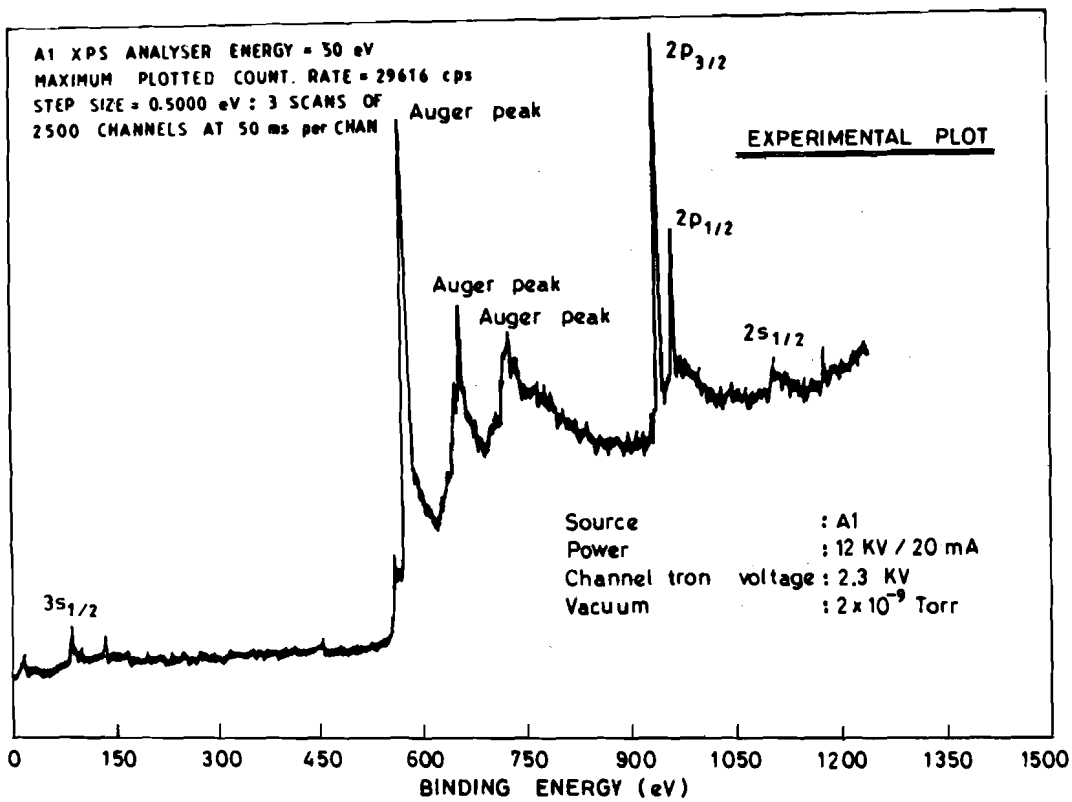

Fig. 3 XPS of copper film

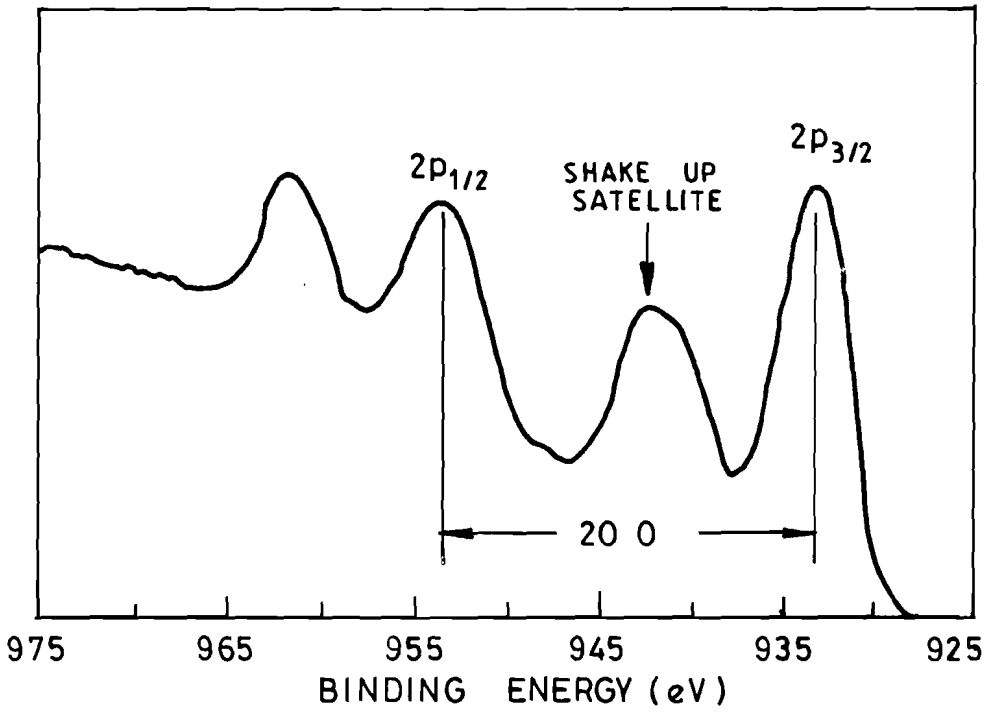

Fig. 4 XPS of bulk copper oxide in the specific energy region (plot from hand book of x-ray and photoelectron spectroscropy)

BASICITY OF A SERIES OF SUBSTITUTED ACETOPHENONES IN GROUND AND SOME LOW-LYING EXCITED STSTES; A THEORETICAL STUDY

D.K. Dinda and B.R.De[**]
Department of Chemistry
Vidyasagar University
Midnapur-721 102, West Bengal, India

Gas phase proton affinities and transition energies of a series of parasubstituted acetophenones in ground state and some low lying excited states have been studied by MNDO calculations with complete geometry optimization of the ground states and relevant excited states. For both ground state and lowest excited singlet state, the gas phase O-protonation turns out to be exothermic and the local stereochemical disposition of the proton is found to be almost the same in each case. The presence of p- substituent is seen to cause very little change of the proton affinities (PA) relative to the unsubstituted acetophenones. Electron releasing p-substituents increase PA values by ~0.3 eV for ground states and ~0.96eV for lowest excited singlet state and electron withdrawing p-substituents decrease it by ~0.51 ev for ground state and ~0.86 ev for lowest excited singlet state. Computed proton affinities are sought to be correlated with a number of computed system parameters eg, the net charge on the carbonyl oxygen atom, (q_0^-), charge on the proton added (q_H+) and the computed hardness (η) of the unprotonated bases in the relevant states. From the PA values it is revealed that the compounds studied are little more basic in the lowest excited singlet state than in the ground state. The computed proton induced shifts (PIS) are, in general, red shifts for the low lying excited states of the para substituted acetophenones. The overall basicity is explained by distant atom contribution in addition to the contribution from the carbonyl group.

Electron donor and acceptor definition of acidity and basicity introduces the idea that there must be some relation between molecular electron density distribution and the acid base properties. This property may also vary from state to state of the same molecule due to some electronic transitions which are accompanied by some extensive reorganization of molecular electronic charge distribution. Basicity of carbonyl molecules in their electronic ground state is well recognised[1-4]. Absorption and fluorescence spectral data in conjunction with Forster cycle[5-7] are utilized for the experimental determination of acid

** Correspondence to Prof. B.R.De.

base properties of molecules in excited states in presence of solvents. Gas phase methods[1,3,8] which ignore the complicating effect of solvation have been successfully applied to determine the gas phase acid-base properties of molecules in excited states. Many reactions of molecules containing carbonyl chromophores are acid catalysed and involve an attack on the carbonyl oxygen by a proton in the primary step.[9-12]. Hydrogen bonding is also very important for the molecules. Systematic experimental data on proton affinities of different carbonyl systems in ground and excited states are scarcely available. Recently the basicities of a series of substituted acetophenones in ground and some low lying excited states have been theoretically calculated[13,14]. The para substituted compounds have been chosen as the case study because the ortho and meta substituted compounds are less stable than para substituted counter parts. The PA values are analysed to understand whether he preprotonation charge distribution local to the chromophore or post protonation relaxation of charge density or both are important in explaining the overall basicity of the acetophenones in a particular state.

The calculations have been performed by the standard LCAO-MO-SCF method at the MNDO level of approximation. For the first excited singlet state (both adiabatic and vertical), only four MO's and 36 configurations were considered in the multielectron configuration interaction calculations. Complete geometry optimization has been carried out on the molecules both before and after protonation. The molecules studied are listed in Table-I along with their respective abbreviated names and computed proton affinities of the ground and first excited singlet state (both adiabatic and vertical). Table-II summarizes the computed net charge on the carbonyl oxygen atoms in the equilibrium ground state and the first excited singlet state of base molecules both before and after protonation. This also includes the net charge carried out by the proton of the protonated bases in the relevant optimized state. The computed net charge on the proton is small in each case and in the range 0.25-0.29 for ground state and 0.24-0.27 for the first excited singlet state showing that a rather large migration of electron density to the added proton has taken place. That this migration is not local and originates from all over the molecule is clearly reflected in the computed net charge on the carbonyl oxygen atom of the protonated bases. The oxygen atom still carries a net negative charge, albeit depleted relative to the unprotonated base in the ground state and in the lowest excited singlet state with the exception of protonated p-nitro acetophenone where it is slightly higher. It is therefore natural to anticipate that the proton affinities of the carbonyl bases cannot be modelled or described by local properties of the carbonyl moiety only. It must be shaped strongly by distant atom contribution in addition to the contribution from the carbonyl group.

Fig.1 plots the computed gas phase proton affinities, PA= ($E^{Total}_{BH^+}$ - E_B), against

the computed net charge density on the carbonyl oxygen atom of the unprotonated bases (q_o-). Fig. 2 shows PA as a function of the computed net charge on the added proton (q_H+) in the fully relaxed B_H+. We have also looked for the existence of correlation with a single global parameter of the entire molecule. As the global parameter we have chosen the hardness, $\eta = (I-A)/2 = (\varepsilon_{LUMO} - \varepsilon_{HOMO})/2$, listed in Table-III. The correlation of PA with η is displayed in Fig.3. All these plots reveal marginal linearity of the computed PA's with respect to the local and global parameters. This indicates that both pre and post-protonation correlations with local charge densities in the immediate neighborhood of the protonation site are weak. Vertical proton affinities also show a more or less similar pattern.

That the local characteristics at or around the >C=O moiety cannot model the substitutent effects is further revealed from the data reported in Table IVa and Ivb, where some of the computed geometrical parameters around the >C=O group are listed. The O-H^+ bond length has a variation in the range 0.95-0.96 A^0 for the ground state and 0.94-0.95 A^0 for the lowest excited singlet state for all the protonated bases. The C-O-H^+ bond angle is ~120^0 for the ground state and in the range 116^0-118^0 for the first excited singlet state and the torsion angle τ (C-C-O-H^+) shows only a small variation $\pm 1^0 - 15^0$ for the first excited singlet state. The carbonyl-ring near invariant stereochemistry around the protonation site of each base tends to suggest that substituent effects to PA cannot be modelled properly unless contributions from far-away centres are taken into account. It also points to the fact that the "local" effects of the group must be very nearly identical in each case. This points to the view that the oxygen lone pair of the carbonyl group is directly involved in the protonation in both the ground state as well as the lowest excited singlet state.

In Table-V the computed transition energies and shifts caused by protonation are shown. This shows four possible transitions.

$^1S_0$ (ground state) $\rightarrow T_1$ (Lowest triplet state)
$^1S_0$ (ground state) $\rightarrow T_2$ (Second lowest triplet state)
$^1S_0$ (ground state) $\rightarrow T_3$ (Third lowest triplet state)
$^1S_0$ (ground state) $\rightarrow S_1$ (Lowest singlet state)

It is clear from the table that in all cases the proton induced shifts (PIS) for the T_1, T_2 and S_1 transitions are red shifts except for the p-nitroacetophenone where it is a blue shift for T_1 and T_2 transitions. For T_3 transitions the PIS are blue shifts for all the molecules. These

data refer to the gas phase protonation of the isolated base molecules without any additional effects caused by solvation.

A perusal of Table-1 reveals that the PA's of all the substituted acetophenones are in the range –6.42(- 6.81) to –7.22(-8.58) eV while that of the unsubstituted base is –6.94(-7.62) eV. In the case of ground state electron releasing substituents are seen to increase the computed PA's while electron withdrawing groups have an opposite effect as expected. Similar is the case with the first excited singlet state with the exception of p-methyl acetophenone. The charge density on oxygen atom before protonation supports the result.

Summing up we see that gas phase O-protonation of acetophenone and its para substituted counterparts is spontaneous in both ground state and in lowest excited singlet state. This is irrespective of electron releasing or withdrawing nature of the para substituent. From Table-1 it is also clear that the compounds studied are little more basic in the first excited singlet state than in the ground state. The overall basicity is explained by distant atom contribution in addition to the contribution from the carbonyl group.

REFERENCES

[1] Beauchamp J.L., Interaction between ions and molecules, Plenum Press, New york, 1974, 413, 459, 489.

[2] Bhome D.K., Mackay G.I., Schiff H.I. and Hemsworth R.S., J.Chem Phys. 1974, 61, 2175.

[3] Brauman J.I. and Blair L.K. J.Am. Chem.Soc. 1970, 92, 5968.

[4] Forster T., Z Electrochem, 1950, 54(42) 1929.

[5] Ottolenghi M., Acc. Chem. Res. 1973, 6,153.

[6] Saeva F.D. and Olin G.R., J.Am. Chem.Soc. 1975,97,5630.

[7] Ireland J.F., and wyatt P.A.H. Adv. Phys. Org. Chem. 1976, 12, 138.

[8] Frieiser B.S., and Beauchamp J.L., J.Am. Chem.Soc. 1977, 99, 3214.

[9] Bhattacharyya S.P., Rakshit S.C., and banerjee M., J.Mol.struc (Theochem), 1983, 91, 253.

[10] Dekock, Jaserse R.L. and Kohin M.S., J.Mol. Struc (Theochem) 1983, 94, 343.

[11] Struszx O.P., Kapny E., Kosmntza C., Robb M.A, Theodrankopoulos G., and Theo. Chem. Acta, 1978,48,215.

[12] Strusz O.P., Kapny E;., Kosmntza C., Robb M.A. and Ciszmadia I.G., Theo. Chem.Acta, 1978, 48, 215.

[13] D.K.Dinda and B.R.De, Ind. J.Chem, 1999, 38B, 657

[14] D.K.Dinda and B.R.De, Ind. J.Chem. 2000 (In Press)

ACKNOWLEDGEMENT

Authors are thankful to CSIR (New Delhi) for the financial support to carry out this work.

Table - I

Computed proton affinities in ground state and in lowest excited Singlet state.

Proton affinity, PA = (E_{BH} + ^{Total} - E_B ^{Total})eV			
Molecule	Ground State	Lowest excited Singlet state	
		Adiabatic	Vertical
A, X = - H	-6.94	-7.62	-7.63
PMA, X = $-CH_3$	-6.98	-7.60	-7.59
PM_yA, X = $-OCH_3$	-7.22	-7.85	-7.28
PAA, X = $-NH_2$	-6.99	-8.58	-8.39
PclA, X = -Cl	-6.76	-7.33	-7.25
PC_uAX = -CN	-6.65	-7.18	-7.13
PNA, X = $-NO_2$	-6.42	-6.81	-6.63

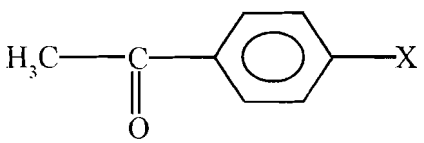

(B)

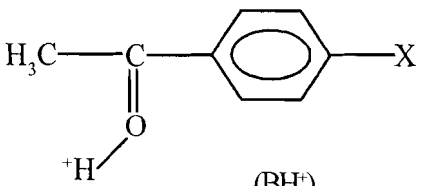

(BH^+)

Table - II (a)

Computed net charge of the ground state

Molecule	Charge on O-atom (q_0-)		Charge on proton (q_H+)
	Before protonation	After protonation	
A	-0.2801	-0.1440	0.2686
PMA	-0.2805	-0.1503	0.2657
PM_yA	-0.2827	-0.1682	0.2541
PAA	-0.2848	-0.1187	0.2860
PClA	-0.2743	-0.1400	0.2706
PC_nA	-0.2723	-0.1351	0.2735
PNA	-0.2644	-0.1041	0.2916

Table - II (b)

Computed net charge of the lowest excited singlet state

Molecule	Charge on O-atom (q_0-)				Charge on proton (q_H+)	
	Before protonation		After protonation			
	Adiabatic	Vertical	Adiabatic	Vertical	Adiabatic	Vertical
A	-0.2802	-0.2793	-0.2527	-0.2614	0.2470	0.2685
PMA	-0.2805	-0.2805	-0.2531	-0.2620	0.2466	0.2657
PM_yA	-0.2834	-0.2825	-0.2279	-0.1483	0.2608	0.2541
PAA	-0.2858	-0.2837	-0.2819	-0.2891	0.2624	0.2866
PClA	-0.2742	-0.2738	-0.2539	-0.2617	0.2552	0.2706
PC_nA	-0.2724	-0.2725	-0.2562	-0.2627	0.2514	0.2735
PNA	-0.2658	-0.2643	-0.2804	-0.2851	0.2705	0.2916

Table - III

Computed hardness, η (eV) of the free base in the ground and lowest excited singlet state.

Molecule	η(ground state)	η(singlet excited state)	
		Adiabatic	Vertical
A	4.802	4.741	4.802
PM_yA	4.697	4.642	4.703
PMA	4.523	4.453	4.521
PAA	4.469	4.370	4.471
PClA	4.684	4.621	4.681
PC_nA	4.602	4.542	4.602
PNA	4.503	4.405	4.501

Table - IV (a)

Computed geometrical features of free base and O-protonated base in ground state (lengths in A^0 and angles in degrees)

Molecule	Free base		O - protonated base		
	r_{C-X}	r_{C-X}	r_{O-H+}	4C-O-H+	4C-C-O-H+
A	1.08	1.09	0.95	109.6	0.5
PMA	1.50	1.51	0.95	119.8	2.2
PM_yA	1.36	1.33	0.95	119.0	1.3
PAA	1.42	1.38	0.96	119.4	-0.1
PClA	1.75	1.74	0.96	119.8	2.1
PC_nA	1.43	1.43	0.96	119.8	2.5
PNA	1.50	1.50	0.96	120.0	0.2

Table IV (b)

Computed geometrical features of free base and O-protonated base in the lowest excited singlet state (lengths in ^{0}A and angle in degrees)

Molecule	Free base				O-protonated base					
	R_{C-X}		R_{C-X}		R_{O-H+}		4C-O-H^{+}		τ(C-C-O-H^{+})	
	Adiabatic	Vertical	Adiabatic	Vertical	Adiabatic	Vertical	Adiabatic	Vertical	Adiabatic	Vertical
A	1.08	1.09	1.09	1.09	0.95	0.95	116.6	119.7	9.2	2.3
PM_yA	1.50	1.50	1.42	1.42	0.94	0.95	116.8	119.8	4.9	2.2
PMA	1.35	1.36	1.29	1.33	0.95	0.95	116.9	119.4	1.9	1.2
PAA	1.39	1.42	1.33	1.38	0.95	0.96	116.2	119.4	-1.2	-0.1
PClA	1.74	1.75	1.72	1.73	0.94	0.96	118.6	119.8	7.8	2.1
PC_nA	1.44	1.41	1.42	1.42	0.95	0.96	116.1	119.8	15.7	2.5
PNA	1.48	1.50	1.51	1.51	0.95	0.96	116.8	120.0	-1.3	0.2

Table - V

Computed transition energies and proton induced shifts (PIS) in the excited singlet state.

Molecule (I_{SO})	State	Transition energies (eV) in Free base		Transition energies (eV) in O-protonated base		Shifts (eV)	
		Adiabatic	Vertical	Adiabatic	Vertical	Adiabatic	Vertical
A	T_1	1.987	2.096	1.683	1.919	-0.304	-0.177
	T_2	2.853	2.946	2.039	2.113	-0.814	-0.833
	T_3	2.873	2.966	3.534	3.591	+0.697	+0.625
	S_1	3.298	3.387	2.525	2.702	-0.773	-0.685
PMA	T_1	1.972	2.090	1.756		-0.216	
	T_2	2.815	2.921	1.962		-0.853	
	T_3	2.841	2.944	3.545		+0.704	
	S_1	3.265	3.364	2.579		-0.785	
PAA	T_1	1.881	2.075	1.248	1.874	-0.663	-0.201
	T_2	2.642	2.864	1.943	2.185	-0.699	-0.679
	T_3	2.674	2.893	2.722	2.826	+0.048	-0.067
	S_1	3.071	3.278	1.288	1.877	-0.1783	0.401
PCIA	T_1	1.984	2.112	1.709	2.020	-0.275	-0.092
	T_2	2.798	2.904	2.125	2.150	-0.673	-0.754
	T_3	2.843	2.952	3.183	3.668	+0.340	+0.716
	S_1	3.266	3.371	2.487	2.876	-0.779	-0.495
PC_nA	T_1	2.047	2.163	1.774	2.021	-0.273	-0.142
	T_2	2.785	2.889	2.122	2.246	-0.663	-0.643
	T_3	2.871	2.974	3.474	3.635	+0.603	+0.661
	S_1	3.294	3.399	2.614	2.863	-0.680	-0.536
PNA	T_1	2.184	2.325	2.241	2.497	+0.057	+0.172
	T_2	2.794	2.933	2.824	3.275	+0.030	+0.342
	T_3	2.904	3.030	4.981	5.017	+1.987	+1.579
	S_1	3.307	3.438	2.709	3.230	-0.598	-0.208

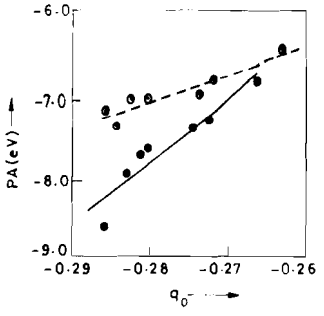

Fig. 1 : Correlation of computed PA with net charge on carbonyl oxygenation (q_O^-). The Θ and—— represent ground state and • and - represent curve for the singlet excited state.

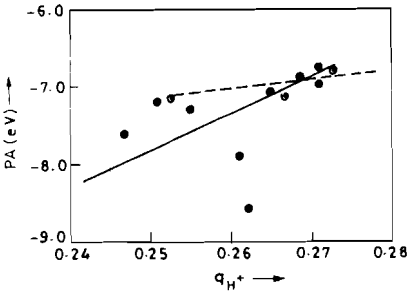

Fig.2 : Correlation of computed PA with net charge on added proton (q_H^+) . The Θ and —— represent ground state and • and – represent curve for the singlet excited state.

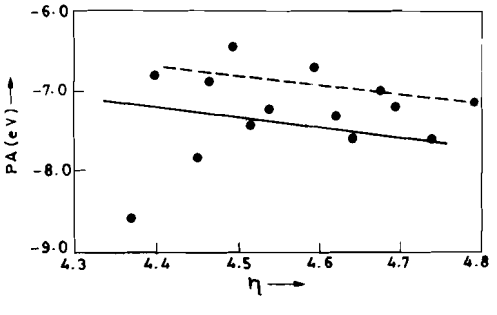

Fig. 3 : Correlation of computed PA with hardness, η. The Θ and —— represent ground state and • and – represent curve for the excited singlet state.

Ni(II) ASSISTED HYDROXYLATION OF PHENYL RING OF 2-(PHENYLAZO) PYRIDINE FORMATION OF 2-(PYRIDYLAZO)-2′-PHENOL

Debasish Manna, Biswaranjan Shee,
Nilkamal Maiti and Surajit Chattopadhyay*.
Department of Chemistry and Chemical Technology
Vidyasagar University
Midnapore-721 102, West Bengal, India

Abstract

Reactivity of $NiL_3(ClO_4)$ [L=2-(phenyl azo) pyridine] toward aqueous hydrogen peroxide have been investigated. The bis chelate, $Ni(OL)_2$, where HOL =2-(pyridylazo)-2-phenol is isolated. The ejected ligand obtained from $Ni(OL)_2$ was identified as HOL.

Key words : Phenylazopyridine, nickel, hydrogen peroxide, hydroxylation.

INTRODUCTION

Chemistry of transition metal chelates incorporating bidentate 2-(arylazo) pyridine ligand has been developed largely in the areas which involve their redox behaviour, [1-14] photophysical properties,[15] and hydroxylation reactions.[16,17] Among the metal mediated hydroxylation reactions in aromatic ring, one notable example is tyrosinase activity in*vivo*, where involvement of copper as a necessary element has been demonstrated.

Herein we describe the hydroxylation of phenyl ring in 2-(phenylazo) pyridine(L) via formation of $NiL_3(ClO_4)$, **1**.

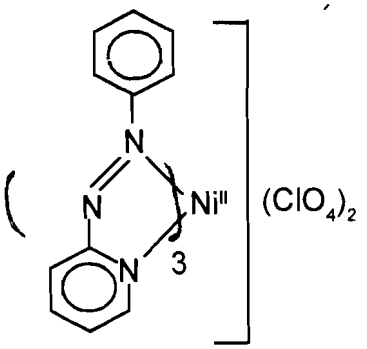

1

Hydroxylation could be achieved by the reaction of aqueous hydrogen peroxide. Conversion of free ligand L→HOL (eq I) by its treatment with hydrogen peroxide, in absence of metal, has not been achieved.

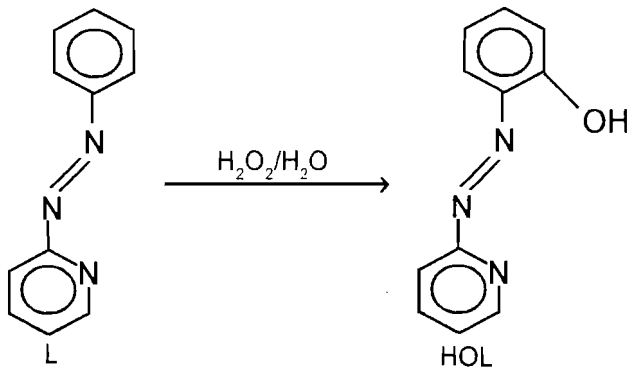

..... (I)

EXPERIMENTAL SELECTION

Materials

Nickel(II) perchlorate was prepared by the reaction of nickel carbonate with perchloric acid. Disodium tetrachloropalladate was prepared by the reaction of palladium(II) chloride with sodium chloride in water and evaporating the aqueous solution as reported earlier[6]. Nitrosobenzene was prepared according to the reported procedure[25]. Commercial grade silica gel(60-120) was used for column chromatography. Sodium hydroxide, acetonitrile, dichloromethane, methanol, benzene and hydrogen peroxide used for the preparative work were of reagent grade. 2-(phenylazo) pyridine ligand was prepared as described earlier.

Physical measurements

UV-Vis and IR spectra were recorded on a Hitachi 330 and Perkin-Elmer 983 spectrophotometers respectively. Micro-analytical data (CHN) were obtained from Perkin-Elmer 240 C analyzer. Magnetic susceptibility were measured on a PAR 155 vibrating sample magnetometer fitted with a walker scientific magnet. ^{1}H-NMR spectra were drawn on BRUCKER 300 MHz.

Synthesis of Tris (2-(phenylazo) pyridine) nickel (II) percholorate, $NiL_3(ClO_4)_2$

Solution of 2-(phenylazo) pyridine (50mg) in methanol was added dropwise to a

magnetically stirred solution of $Ni(ClO_4)_2.6H_2O$(330 mg) in methanol. The reaction mixture was stirred for ½ hr . The colour of the reaction mixture was dark green. The mixture was kept over night at room temperature. The dark green crystals formed were filtered and washed with little methanol and dried. Yield was 0.41g.

Anal. Calcd. For $C_{33}H_{27}N_9C_{12}O_8Ni$: C,49.9 ; N , 15.65 ; H , 3.35.

Found . C , 50.02 ; N ,15.10 ; H , 3.55.

Reaction of $NiL_3(ClO_4)_2$ with hydrogen peroxide: Formation of Ni (OL) $_2$

10 ml of 30 % hydrogen peroxide was added dropwise to a stirred solution of $NiL_3(ClO_4)_2$ (500 mg) in 25ml of acetonitrile and stirring was continued for 12 hr. Acetonitrile was evaporated at room temperature . The violet complex was extracted with dichloromethane followed by evaporation to dryness at room temperature . The solid residue thus obtained was subjected to chromatography on silica gel using mixture of acetonitrile and benzene (6:4 v/v) as eluent . The violet band was collected to obtain the desired product.

Yield = 0.07 g. Anal. Calcd. For $C_{22}H_{16}N_6O_2Ni$:C, 57.76; N 18.38 ; H , 3.50 .

Found.C ,58.10 ; N , 19 . 10 ; H , 3.20 .

Isolation of hydroxylated ligand (HOL):

To the solution of $Ni(OL)_2$ (0.5 g) in 5ml of dichloromethane 0.01 M perchloric acid in acetonitrile was added dropwise. A light orange liquid was obtained which was violet previously. The solution was evaporated and extracted with dichloromethane. The extract was then subjected to column chromatography on silica gel column .The first orange band was collected. The eluent was acetonitrile and benzene (3:7 v/v) mixture. Yield was 0.14gm.

Synthesis of Pd (OL) Cl:

250mg hydroxylated Ligand (LOH) was added dropwise to a stirred solution of Na_2PdCl_4 (300mg) in 5ml methanol and stirring was continued for 6 hrs. Methanol was evapourated at room temperature. Green compound Pd (OL) Cl was obtained and was purified by column chromatography. Yield, 0.32gm.

RESULTS AND DISCUSSION

The green compound , Ni L_3 $(ClO_4)_2$ was synthesized by the reaction of L with $Ni(ClO_4)_2.6H_2O$ in methanol .[1] The complex was characterized by matching the physical properties with that of the reported one.[1]

Green NiL_3 $(ClO_4)_2$ afforded a violet solution upon treatment with 30% hydrogenperoxide at room temperature. Upon evaporation of solvent a dark solid was obtained which was subjected to column chromatography on silica gel column. A yellow band was first eluted out with benzene followed by a violet band with acetonitrile –benzene mixture. The compound obtained from the yellow band was identified as the ligand, L. The violet band afforded a blue solid where no vibrations for perchlorate ion in the IR spectrum was observed (Fig-1.) Uv-Vis spectrum (Fig-2, Table-1) showed an absorption at 850 nm (ε=100 M^{-1} Lit cm^{-1}). UV-Vis spectrum of a reported complex with tridentate (O,N,N)

Fig.1, Fig.2; see pages 50, 51

ligand has absorption at 790 nm (ε=240 M^{-1} Lit. cm^{-1}).[27] Magnetic susceptibility data (μ_{eff} ≈ 3.00 B.M.) corresponds to two unpaired electrons. The elemental analysis data is well in agreement with the proposed composition , $Ni(OL)_2$, **2**, where OL^- is the anion of HOL. The preformed ligand, **3,** forms a bis complex with Ni(II) where the Ligand span in a

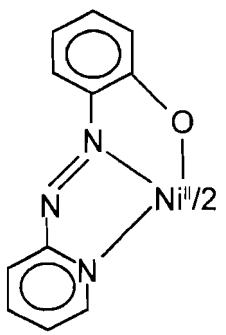

2

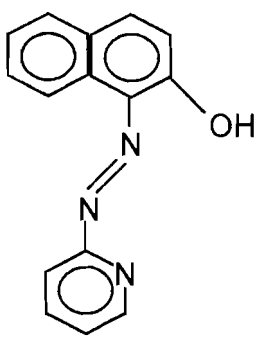

3

meridional fashion[27]. In $Ni(OL)_2$, the coordination mode of the ligand is proposed to be of similar kind by analogy. Therefore in $Ni(OL)_2$ each ligand is bound to the metal ion in a meridional fashion.

To identify the HOL it was necessary to obtain the free ligand. For this purpose the ligand was isolated by treating $Ni(OL)_2$ with 0.01M perchloric acid in acetonitrile and purified by column chomatography over silica gel column. The purified ligand, HOL, has distinctly different absorption spectrum to that of L(Fig-3,Table-1).

Fig-3, see page- 52 ; Table-1, see page - 49

In the ^{1}H-NMR spectrum, a resonance at 12.87δ was observed which vanished upon shaking with D_2O indicating presence of phenolic OH in the ligand[23]. Reaction of HOL with Na_2PdCl_4 in methanol afforded a green compound. The electronic spectral data (Table-1) of this green compound matched with Pd(OL)Cl,**4**, which is reported elsewhere [17]. Formation of

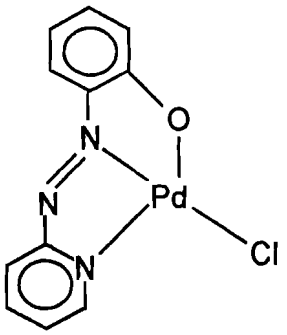

4

Pd(OL)Cl can be regarded as an evidence in support of the site of hydroxylation in the ligand fragment.

CONCLUSION

$NiL_3(ClO_4)$ affords a bis chelate $Ni(OL)_2$ upon treatment with hydrogen peroxide in aqueous acetonitrile at room temperature. The metal oxidation state remained unaltered after the reaction. The hydroxylated ligands has been characterised after isolating in pure form . ^{1}H-NMR spectrum of the ligand showed a resonance at 12.87 δ, which vanishes upon shaking with D_2O , indicative of free –OH (phenolic). Formation of Pd(OL)Cl upon reaction with Na_2PdCl_4 also supports the formation of hydroxylated ligand, HOL.

ACKNOWLEDGEMENT

We are grateful to RSIC (NEHU) for drawing ^{1}H-NMR and IR spectra. Prof. M.K.Chaudhuri's help in every step of this work is acknowledged. We are thankful to Prof. S.N.Bhat for drawing the UV-Vis spectra. We acknowledge the financial support of Council of Scientific and Industrial Research, New Delhi.

REFERENCES

[1] B . S .Raghavendra and A. Chakraborty, *Ind. J. Chem..*, 1976, **14A**, 166.
[2] S. Goswami, A. R. Chakravarthy and A. Chakraborty, *Inorg. Chem.*,1981 **20**, 2246.
[3] S.Goswami, A. R. Chakravarthy, *Inorg. Chem.* 1983, **22**, 602.
[4] S. Goswami, R. N. Mukherjee and A. Chakravorty, *Inorg. Chem.* 1983, **22**, 2285.
[5] P. Ghosh and A. Chakravorty, *J. Chem. Soc. Dalton Trans.*, 1985, 361.
[6] S.Goswami, A. R. Chakravarthy and A. Chakravorty *Inorg. Chem*,1982,**21**,2731.
[7] A.K.Deb, M.Kakoti and S.Goswami , *J. Chem. Soc. Dalton Trans.*,1991,3249.
[8] B.K.Ghosh, A.Mukhopadhyay, S.Goswami and A.Chakravorty,*Inorg.Chem.*, 1984,**23**,4633.
[9] B.K.Ghosh, S.Goswami and A. Chakravorty, *Inorg.Chem*,1983,**22**,3358.
[10] D.Dutta and A. Chakravorty, *Inorg.Chem* ,1983,**22**,1085.
[11] R.A.Krause and K.Krause, *Inorg.Chem*, 1980,**19**,2600.
[12] R.A.Krause and K.Krause, *Inorg.Chem*, 1982,**21**,1714.
[13] M.N.Ackerman,C.R.Barton,C.J.Doedens,E.M.Speeht, S.C.Keill,W.E.Schreiber and H.Kim, *Inorg.Chem*, 1989,**28**,397.
[14] T.K.Mallick, P.K.Das, B.K.Roy and B.K.Ghosh, *Trans.Met.Chem.*, 1993,**18**,609.
[15] M.Kakoti, A.K.Deb and , S.Goswami, *Inorg.Chem*, 1992,**31**,1302.
[16] A.K.Mahapatra, D Bandyopadhyay, P. Bandyopadhyay, and A. Chakravorty, *Inorg.Chem*, 1986, 252, 2214.
[17] C.K.Pal, S. Chattopadhyay, C.Sinha, D Bandyopadhyay and A.Chakravorty, *Polyhe dron*,1994,**13**,999.
[18] D.Hayaishi (Ed) Molecular Mechanism of Oxygen Activation, *P.I.Academic Press*, New York (1974).
[19] G.H. Hamilton , in Molecular Mechanism of Oxygen Activation, P.405, *Academic Press*, New York (1974).
[20] R.A.Sheldon and J.K.Kochi,Metal –Catalysed Oxidation of Organic Compounds, P.236, , *Academic Press*, New York (1981).
[21] C.Sinha, D Bandyopadhyay and A. Chakravorty, *Inorg.Chem*, 1988,**27**,1173.

[22] C.K.Pal , S. Chattopadhyay, C.Sinha, and A. Chakravorty, *J.Organomet. Chem.*,1992,439,91.
[23] S.Chattopadhyay, C.Sinha, S.B. Choudhury and A. Chakravorty, *J.Organomet.* Chem.,1992,427,111.
[24] M.Sarwar Nasir, B.I.Cohen and K.D.Karlin, *Acc. Chem. Res.*, ,1991,**24**,1and references therein.
[25] A.I.Vogel ,*Practical Org. Chem.*, P.689.
[26] K.Nakamoto,*IR and Raman Spectra of Inorg.and Coordination Compounds 4th. Ed.,John Willey*, 1936,P.251.
[27] D.Roy, S.Mukhopadhyay, *J Chem. Soc. Dalton Trans* .,1995,265.

Table - 1

UV-Vis, IR and magnetic moment data

Compound	UV-Vis[a] λ,nm (dm ^{3} M $^{-1}$ cm $^{-1}$)	IR [b] ν (cm $^{-1}$)	μ_{eff}
L	440(4203), 320(21,000)	1617, 1582, 1477, 1421, 687	.....
$NiL_3(ClO_4)_2$	950 (12), 600 (350), 340 (32000).	1602, 1586, 1473, 1446, 1431, 769, 692, 1115.	2.77
$Ni(OL)_2$	850 (100), 570 (17100), 540 (14545), 370 (18181), 310 (16363).	1597, 1480, 1447, 1382, 1365.	3.00
Pd(OL)Cl	710 (5550), 660 (6650), 620 (4500), 370 (20000), 360 (17000).	.....	.....
LOH	380 (3184), 320 (20000).	1579, 1482, 1458, 1417, 792, 686.	.....

[a]In dichloromethane solution at 298K. [b]In KBr disc. [c]Shoulder.

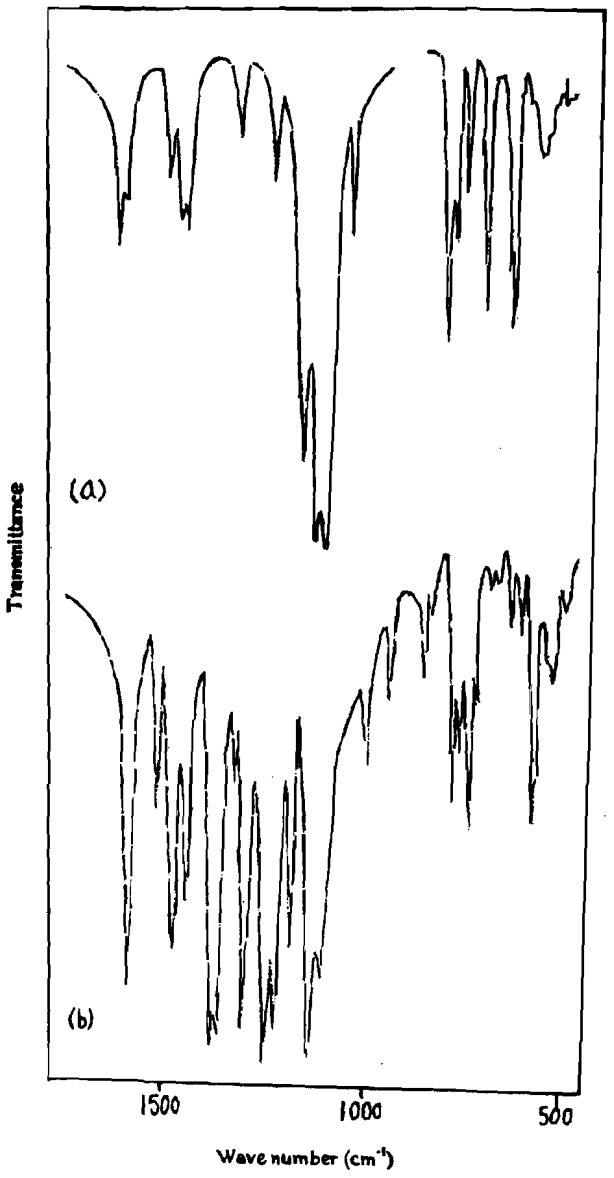

Figure 1 : IR spectra of (a) $NiL_3(ClO_4)_2$ and (b) $Ni(OL)_2$

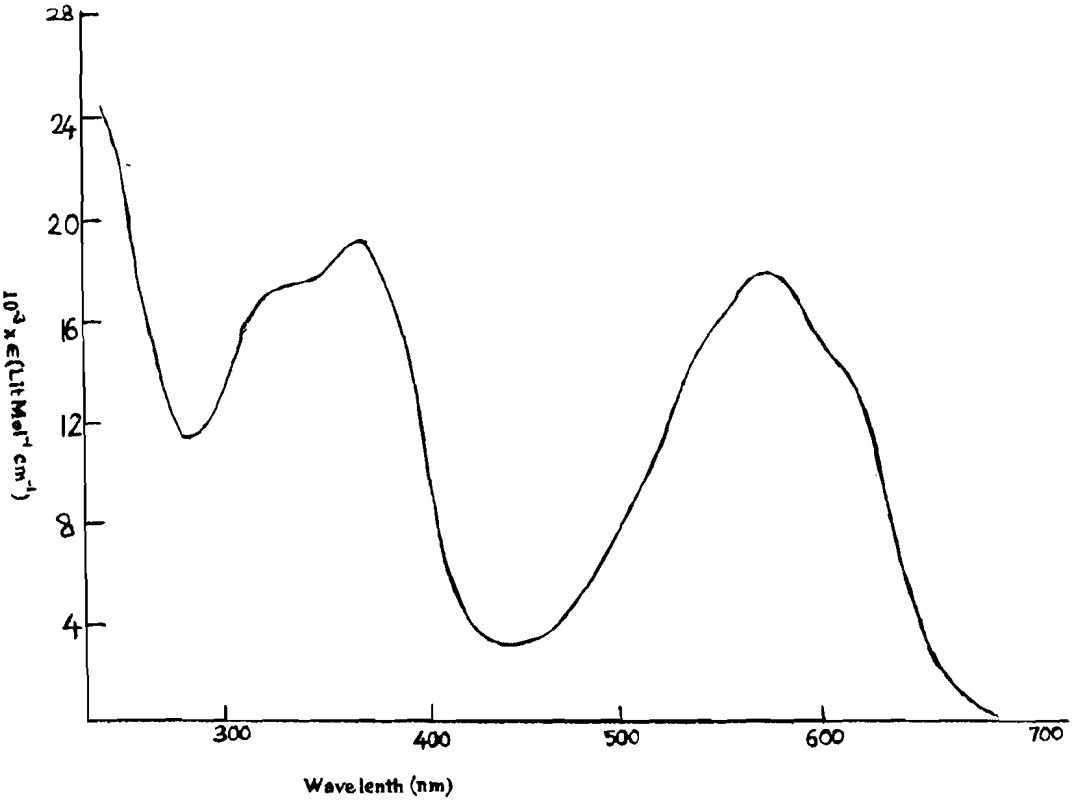

Figure 2 : Uv-vis spectrum of $Ni(OL)_2$

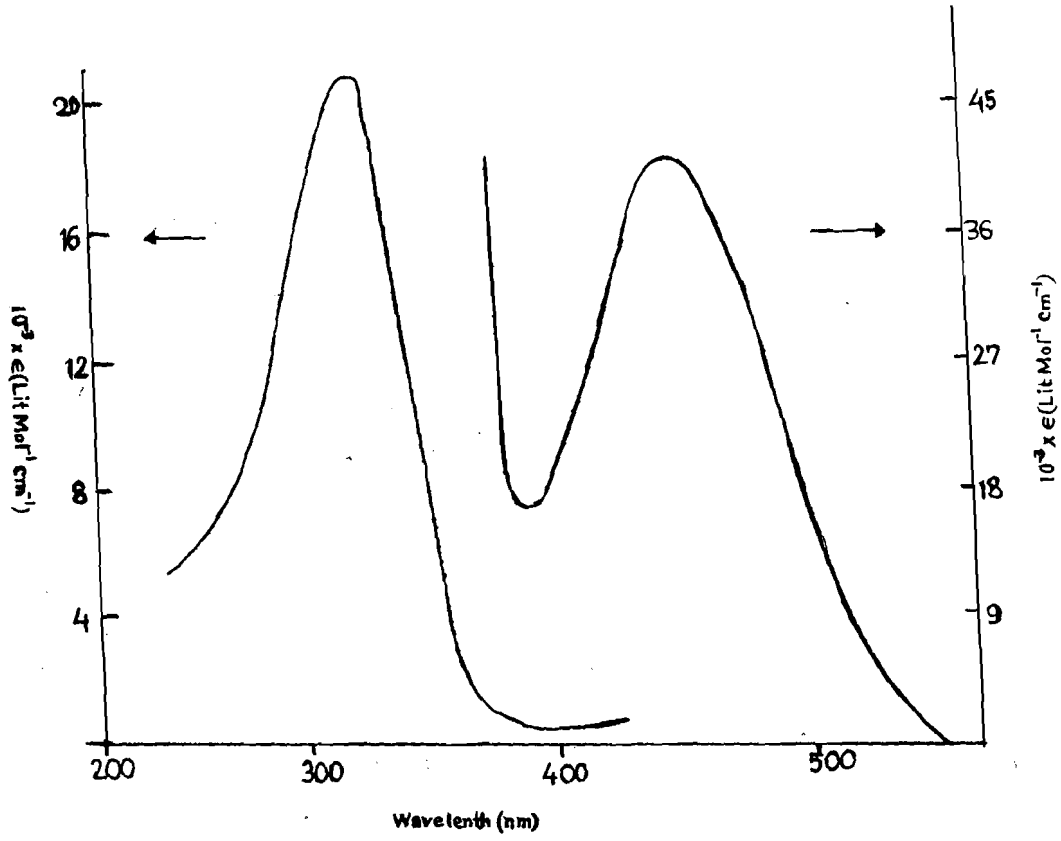

Figure 3 : Uv-vis spectrum of HOL

DETERMINATION OF KINETIC PARAMETERS IN DIFFERENTIAL THERMAL ANALYSIS

Manabesh Bhattacharya[a], W. G. Devi[b] and S. D. Singh[c]
[a]Department of Physics, Krishnath College,
Berhampore - 742 101, Murshidabad, West Bengal, India
[b]Department of Chemistry, T. S. Paul Manipur Womens' College
Monsangei, Imphal - 795 008, Manipur, India
[c]Department of Physics, School of Science,
Manipur University, Chanchipur, Imphal - 795 003, Manipur, India

Abstract :
A method is suggested for the determination of the kinetic parameters in differential thermal analysis by using the points of inflection of the differential thermal analysis curve. The possibility of the determination of the temperature exponent of the pre-exponential factor is also considered.

Key words : Differential thermal analysis, order of kinetics, activation energy, preaexponential factor.

INTRODUCTION

Differential thermal analysis (DTA) is a non-isothermal thermoanalytical technique which has been widely used in the analysis of different types of reactions [1, 2]. DTA finds applications in a number of areas such as the identification of various types of materials, the studies of properties like thermal stability etc. Luo et al [3] presented a method of analysis of DTA curve by using its points of inflection. But he has not taken into account the temperature dependence of pre-exponential factor. It is to be noted that the application of integral methods in non-isothermal kinetics of solid state reactions usually assumes the temperature independence of pre-exponential factor in Arrhenious equation namely [1, 2]

$$k = A\exp(-E/RT) \qquad (1)$$

where k is the specific reaction rate, R is the universal gas constant, T is the temperature and E is the activation energy. In reality it is only possible to express A as a function of

temperature as [4-9]

$$A = A_r T^r \tag{2}$$

where $-2 \leq r \leq 2$. In the present paper we have developed a method for the determination of kinetic parameters from a DTA curve by using its points of inflection by taking $-2 \leq r \leq 2$. We test the applicability of the method by applying it to computer generated and experimental DTA curves. Furthermore, a method of evaluation of temperature exponent r is also presented.

THEORY

Following Luo et al [3] the expression for the solid state decomposition reaction of nth order can be expressed as

$$\frac{dx}{dt} = A(1 - x)^n exp(- E / RT) \tag{3}$$

where x is the fraction of the reaction completed in time t. Using equation (2), equation (3) can be written as

$$\frac{dx}{dt} = A_r T^r (1 - x)^n exp(- E / RT) \tag{4}$$

In a DTA curve the temperature deviation ΔT from the horizontal base line can be expressed via equation (4) as

$$\Delta T = \beta A_r T^r [1 + (n - 1)\frac{A}{\phi}\int_{T_0}^{T} T'^r \, exp(- E / RT')dT' \times exp(- E / RT) \quad (for\ n \neq 1) \tag{5}$$

and

$$\Delta T = \beta A_r T^r exp[- \frac{A}{\phi}\int_{T_0}^{T} T'^r \, exp(- E / RT')dT']e^{(-E/RT)} \quad (for\ n = 1) \tag{6}$$

where ϕ is the linear heating rate, T_0 is the initial temperature, T is the temperature at time t and β is a proportionality constant. Following Gartia et al [10] the integral $\int_{T_0}^{T} T'^r exp\,(- E / RT')dT'$ occuring in equation (5) and (6) can be written as

$$\int_{T_0}^{T} T'^{r} \exp(-E/RT')dT' = (E/R)^{r+1}[\Gamma(-r-1, u) - \Gamma(-r-1, u_0)] \quad (7)$$

with $u = \frac{E}{RT}$ and $\Gamma(r, u)$ is the complementary incomplete Gamma function [11].

The peak temperature T_m of the DTA curve can be obtained from the equation

$$\left[\frac{d(\Delta T)}{dT}\right]_{T=T_m} = 0 \quad (8)$$

From equations (5) and (6) the peak temperatures T_m of a first order (n = 1) and non-first order ($n \neq 1$) DTA curves can be obtained as

$$\frac{E}{RT_m^2} - n\frac{A_r T_m^r}{\phi}\exp(-\frac{E}{RT_m})[1 + \frac{A_r(n-1)}{\phi}\int_{T_0}^{T_m} T'^{r}\exp(-E/RT')dT']^{-1} + \frac{r}{T_m} = 0 \quad (9)$$

From equations (5), (6), (8) and (9) we get

$$\frac{\Delta T}{(\Delta T)_m} = (\frac{u_m}{u})^r \exp[u_m - u + F(u, u_m)] \; (n = 1) \quad (10)$$

and

$$\frac{\Delta T}{(\Delta T)_m} = (\frac{u_m}{u})^r \exp(u_m - u)[1 - \frac{n-1}{n}F(u, u_m)]^{-\frac{n}{n-1}} \quad (n \neq 1) \quad (11)$$

with

$$F(u, u_m) = (ru_m + u_m^2)u_m^r \exp(u_m)[\Gamma(-r-1, u_m) - \Gamma(-r-1, u)] \quad (12)$$

$(\Delta T)_m$ in the above equations denotes the value of ΔT at peak temperature T_m. The inflection points T_{i1} and T_{i2} with rising and falling sides of a DTA peak can be obtained from the equation

$$\frac{d^2(\Delta T)}{dT^2} = 0 \quad (13)$$

To a good approximation the relation between u_m and $u_x u_y/(u_m|u_x - u_y|)$ (where u_x and u_y correspond, respectively, to the values of u at the points of inflection and / or at the peak temperature) is found to be linear so that

$$u_m = \frac{C_1 u_{i1}}{(u_{i1} - u_m)} + D_1 \quad (14)$$

$$u_m = \frac{C_2 u_{i2}}{(u_m - u_{i2})} + D_2 \quad (15)$$

$$u_m = \frac{C_3 u_{i1} u_{i2}}{u_m(u_{i1} - u_{i2})} + D_3 \quad (15)$$

where $u_{i1} = \frac{E}{RT_{i1}}$ and $u_{i2} = \frac{E}{RT_{i2}}$. Equations (14) - (16) can be finally expressed as

$$E_1 = \frac{C_1 RT_m^2}{(T_m - T_{i1})} + D_1 RT_m \quad (17)$$

$$E_2 = \frac{C_2 RT_m^2}{(T_{i2} - T_m)} + D_2 RT_m \quad (18)$$

$$E_3 = \frac{C_3 RT_m^2}{(T_{i2} - T_{i1})} + D_3 RT_m \quad (19)$$

The co-efficients C_j and D_j (j = 1 -3) depend both on r and n. For a particular value of n one can write

$$C_j = c_{oj} + c_{ij} r \quad (20)$$

$$D_j = d_{oj} + d_{ij} r \quad (21)$$

Again it has been found that the ratio $R_{ij} = \frac{(\Delta T)_{T=T_{ij}}}{(\Delta T)_{T=T_m}}$ (j = 1, 2) where T_{i1} and T_{i2} are the temperatures corresponding to the point of inflection depends strongly on n, weakly on $u_m = E / RT_m$ and is almost independent of the temperature exponent r. For $u_m \geq 40$, R_{ij} is practically independent of u_m and by using the standard technique of non-linear regression [12] can be expressed as

$$R_{i1} = 0.7663 - 0.0904n + 0.0155n^2 \quad (22)$$

$$R_{i2} = 0.1068 + 0.5221n - 0.1141n^2 \quad (23)$$

Equations (22) and (23) can be used to estimate the order of kinetics (n) of a DTA peak.

RESULTS AND DISCUSSIONS

The equation (13) for the determination of the temperatures T_{i1} and T_{i2} corresponding to the points of inflection of a DTA peak have been solved numerically by using New-

ton - Raphson method (see Appendix). In this connection we have used the computer code developed by Mathews [13]. It is to be noted that Newton-Raphson method is very much sensitive to the initial guess value of T_{i1} and T_{i2} . Mathews [13] has also prescribed a programme for the approximate determination of the initial guess values. It may be pointed out here that the complementary incomplete Gamma function occuring in $F(u, u_m)$ [Eq. (12)] has been evaluated by using the continued fraction method [14]. The coefficients c_{ij} and d_{ij} occuring in equation (20) and (21) have been evaluated by employing a rigorous computer code of linear regression developed by Singh [12]. Coefficients c_{ij} and d_{ij} have been depicted in Table 1.

Now we apply the present method to determine the kinetic parameters of some computer generated DTA peaks. The activation energies of those peaks as calculated by using equations (17) - (19) are presented in Table 2. The corresponding value of the order of kinetic are displayed in Table 3. n_1 and n_2 denote, respectively, the values of the order of kinetics as obtained from equations (22) and (23). It is seen that the calculated value of E and n for the computer generated DTA peaks are in fair agreement with their input values.

We now consider the experimental DTA curve [14, 15] of the dehydration reaction $Ni(mpipz)_2(NCS)_2.2H_2O \rightarrow Ni(mpipz)_2(NCS)_2$, where mpipz stands for N-methylpiperazine recorded with two different heating rates namely $\phi = 5^0C / min$ and $\phi = 10^0C / min$. This DTA curve corresponding to $\phi = 5^0C / min$ has been analysed by Singh and Mitra [15] in the framework of Borchardt and Daniels method [16]. The point of inflection have been evaluated by using the cubic spline method [13].

In Table 4 we present the kinetic parameters E_p (activation energy), n_p (order of kinetics) obtained by the present method together with the value E_{BD} of the activation energy as calculated by Borchardt and Daniels method [16]. It is to be noted that, n_p is the average of the values n_1 and n_2 obtained from equations (22) and (23) and E_p is the average of the values E_1, E_2 and E_3 as calculated from equations (17) - (19). Knowing n_p and E_p, pre-exponential factor A_p can be calculated from equations (10) and (11) provided temperature exponent r is known. We have already seen that r cannot be determined from equations (22) and (23) because the ratios R_{i1} and R_{i2} are almost independent of r.

In order to remove this difficulty we follow a method outlined by Townsend and Kelly [17]. In this method the DTA curve is to be recorded for two different heating rates resulting in two different sets of temperatures (T_m, T'_m), (T_{i1}, T'_{i1}) and (T_{i2}, T'_{i2}). Now from equations (17) - (19) we get

$$r = - \frac{c_{01}F_1 + d_{01}G}{c_{11}F_1 + d_{11}G} \qquad (24)$$

$$r = - \frac{c_{02}F_2 + d_{02}G}{c_{12}F_2 + d_{12}G} \qquad (25)$$

$$r = - \frac{c_{03}F_3 + d_{03}G}{c_{13}F_3 + d_{13}G} \tag{26}$$

with

$$G = T_m - T'_m \tag{27}$$

$$F_1 = \frac{T_m^2}{(T_m - T_{i1})} - \frac{T'^2_m}{(T'_m - T'_{i1})} \tag{28}$$

$$F_2 = \frac{T_m^2}{(- T_m + T_{i2})} - \frac{T'^2_m}{(- T'_m + T'_{i2})} \tag{29}$$

$$F_3 = \frac{T_m^2}{(T_{i2} - T_{i1})} - \frac{T'^2_m}{(T'_{i2} - T'_{i1})} \tag{30}$$

Now we can apply the expressions (24) - (26) to the experimental DTA curve mentioned above because it has been recorded with two different heating rates. We denote the value of r as calculated from equations (24), (25) and (26), respectively, by r_1, r_2 and r_3 and present them in Table 5. Keeping in mind that the experimental errors which are likely to creep in we can say that the experimental DTA peak considered here nearly corresponds to the case of the temperature independent pre-exponential factor that is r = 0. Now knowing E_p, n_p and r the pre-exponential factor A_p can be evaluated either from equation (10) or (11) and is also presented in Table 5. It is seen that E_p and E_{BD} are close to each other and the present method also gives other kinetic parameters namely pre-exponential factor and order of kinetics.

CONCLUSION

In the present paper we have developed a method for the determination of kinetic parameters from DTA by using the points of inflection of the DTA curve for the case when the pre-exponential factor is temperature dependent. We have tested the suitability of the method by applying it both to computer generated and experimental DTA curves. We have attempted to determine the temperature exponent by following the suggestion of Townsend and Kelly [17].

ACKNOWLEDGMENTS

The authors are grateful to Professor P. D. Townsend for his suggestions.

REFERENCES

[1] R. Chen and Y. Kirsh, Analysis of Thermally Stimulated Processes, Pergamon, Oxford (1981), Chapter 4.

[2] W. W. Wendlandt, Thermal Method of Analysis, Wiley, New York, 1974.

[3] K. M. Luo, Thermochim. Acta, **255** (1995) 241.

[4] E. Urabanovici and E. Segal, Thermochim. Acta, **168** (1990) 71.

[5] J. E. House, Jr., Thermochim. Acta, **48** (1981) 165.

[6] J. E. House, Jr. and J. Daniel House, Thermochim. Acta, **54** (1982) 213.

[7] M. Balarin, J. Computational Phys., **57** (1985) 26.

[8] D. Dollimore, G. A. Garden and T. J. Taylor, Thermochim Acta **54** (1982) 181.

[9] R. Chen, J. Mater. Sc. **11** (1976) 1521.

[10] R. K. Gartia, S. D. Singh, T. J. Singh and P S Mazumdar, J. Thermal Anal. **42** (1994) 1001.

[11] M. Abramowitz and I. A. Stegan (Eds.), Hand.Book of Mathematical Functions, Dover, New York (1965).

[12] S. J. Singh, Ph. D. Thesis, Manipur University, India, 1992.

[13] J. H. Mathews, Numerical Methods for Mathematics, Science and Engineering, Prentice Hall, New Delhi, 1994.

[14] W G Devi Vidyasagar University Journal of Physical Sciences **3** 18 (1997)

[15] L. K. Singh and S. Mitra, J. Chem. Soc. Dalton Trans. p.2089 (1987).

[16] H. J. Borchardt and F. Daniels, J. Am. Chem. Soc. **79** (1957) 41.

[17] P. D. Townsend and J. C. Kelley, Colour Centers in Solids, Cambridge University Press, Cambridge (1981).

APPENDIX

Numerical evaluation of the points of inflection of a DTA curve for the case of temperature dependent pre-exponential factor.

Using equations (10) - (12), equation (13) can be expressed as

$$f(u) = 0 \tag{31}$$

with

$$f(u) = 2\frac{d(\Delta T)}{du} + u\frac{d^2\Delta T}{du^2} \tag{32}$$

where

$$\frac{d(\Delta T)}{du} = \Delta T\left(\frac{dF}{du} - \frac{r}{u} - 1\right) \quad (n = 1) \tag{33}$$

$$\frac{d(\Delta T)}{du} = -\Delta T\left(\frac{r}{u} + 1\right) + \frac{u_m r}{u} exp(u_m - u)\left(\frac{dG}{du}\right) \quad (n \neq 1) \tag{34}$$

$$\frac{d^2(\Delta T)}{du^2} = \Delta T\left(\frac{d^2F}{du^2} + \frac{r}{u^2}\right) + \frac{d\Delta T}{du}\left[\frac{dF}{du} - \frac{r}{u} - 1\right] \quad (n = 1) \tag{35}$$

$$\frac{d^2(\Delta T)}{du^2} = -\frac{d(\Delta T)}{du}\left(\frac{r}{u} + 1\right) + \frac{r\Delta T}{u^2} + \frac{u_m r}{u} exp(u_m - u)\left[-\frac{dG}{du}\left(\frac{r}{u} + 1\right) + \frac{d^2G}{du^2}\right] \quad (n \neq 1) \tag{36}$$

In the above equations

$$G = D^{-\frac{n}{n-1}} \tag{37}$$

$$D = 1 - \frac{n-1}{n} F(u, u_m) \tag{38}$$

For different values of $u_m (= E / RT_m)$ the values of $u_{ij} (= E / RT_{ij})$ corresponding to the two points of inflection can be found by solving equation (31) numerically with Newton-Raphson method [13] according to which

$$u_{ij}^{k+1} = u_{ij}^{k} - \frac{f(u_{ij}^{(k)})}{\left(\frac{df}{du}\right)_{u = u_{ij}^{(k)}}} \tag{39}$$

where $u_{ij}^{(k)}$ is the kth approximation to u_{ij}. The starting values $u_{ij}^{(0)}$ of u_{ij} have been generated

by using the computer code suggested by Mathews [13]. Now from equation (32)

$$\frac{df}{du} = u\frac{d^3(\Delta T)}{du^3} + 3\frac{d^2(\Delta T)}{du^2} \tag{40}$$

with

$$\frac{d^3(\Delta T)}{du^3} = \frac{d^2(\Delta T)}{du^2}\left(\frac{dF}{du} - \frac{r}{u} - 1\right) + 2\frac{d(\Delta T)}{du}\left[\frac{d^2F}{du^2} + \frac{r}{u^2}\right] + \Delta T\left[\frac{d^3F}{du^3} - \frac{2r}{u^3}\right] \quad (n=1) \tag{41}$$

$$\frac{d^3(\Delta T)}{du^3} = -\frac{2r\Delta T}{u^3} + \frac{2r}{u^2}\frac{d(\Delta T)}{du} - \left(1 + \frac{r}{u}\right)\frac{d^2(\Delta T)}{du^2} + \left(\frac{u_m}{u}\right)^r exp(u_m - u)$$

$$\left[\frac{d^3G}{du^3} - 2\left(1 + \frac{r}{u}\right)\frac{d^2G}{du^2} + \left\{\left(1 + \frac{r}{u}\right)^2 + \frac{r}{u^2}\right\}\frac{dG}{du}\right] \tag{42}$$

Using the integral representation of the incomplete Gamma function [11] namely

$$\Gamma(-r-1, u) = \int_u^\infty exp(-u')u'^{-r-2}du' \tag{43}$$

and the relation [11]

$$\frac{d\Gamma}{du} = -exp(-u) / u^{r+2} \tag{44}$$

one gets

$$\frac{dF}{du} = (u_m^2 + ru_m)\frac{u_m r}{u} exp(u_m - u) / u^2 \tag{45}$$

$$\frac{d^2F}{du^2} = -\frac{dF}{du}\left\{1 + \frac{r+2}{u}\right\} \tag{46}$$

$$\frac{d^3F}{du^3} = -\frac{d^2F}{du^2}\left(1 + \frac{r+2}{u}\right) + \frac{dF}{du}\frac{r+2}{u^2} \tag{47}$$

Table 1 : **Coefficients c_{ij}, d_{ij} occuring in equations (20) and (21).**

n	j	c_{0j}	c_{1j}	d_{0j}	d_{1j}
0.7	1	8.144(-1)	-1.255(-4)	-1.504(-1)	-9.878(-1)
0.7	2	8.141(-1)	-8.214(-5)	-2.112(-1)	-9.911(-1)
0.7	3	1.629	-2.073(-4)	-1.808(-1)	-9.895(-1)
1.0	1	9.628(-1)	-2.618(-4)	-5.633(-1)	-9.758(-1)
1.0	2	9.6262(-1)	-2.578(-4)	-6.981(-1)	-9.750(-1)
1.0	3	1.925	-5.189(-4)	-6.300(-1)	-9.754(-1)
1.5	1	1.159	-4.780(-4)	-1.175	-9.601(-1)
1.5	2	1.159	-5.347(-4)	-1.437	-9.545(-1)
1.5	3	2.317	-1.010(-3)	-1.305	-9.574(-1)
2.0	1	1.316	-6.758(-4)	-1.719	-9.477(-1)
2.0	2	1.316	-7.590(-4)	-2.098	-9.397(-1)
2.0	3	2.632	-1.429(-3)	-1.906	-9.439(-1)
2.5	1	1.448	-8.522(-4)	-2.209	-9.374(-1)
2.5	2	1.447	-9.285(-4)	-2.692	-9.291(-1)
2.5	3	2.896	-1.771(-3)	-2.448	-9.335(-1)
3.0	1	1.563	-1.009(-3)	-2.658	-9.288(-1)
3.0	2	1.561	-1.046(-3)	-3.233	-9.215(-1)
3.0	3	3.124	-2.045(-3)	-2.941	-9.254(-1)

Table 2 : **Activation energies of some computer generated DTA peaks.**

n	E_m (KJ/mole)	T_m (K)	r	R_{i1}	R_{i2}	E_1 (KJ/mole)	E_2 (KJ/mole)	E_3 (KJ/mole)
1.0	41.842	151.4703	0	0.693	0.531	41.834	41.838	41.836
1.0	41.842	119.1050	2	0.697	0.528	41.847	41.849	41.848
1.0	41.842	216.1861	-2	0.683	0.538	41.827	41.831	41.829
1.5	41.842	151.3532	0	0.668	0.631	41.844	41.846	41.845
1.5	41.842	119.0522	2	0.672	0.627	41.859	41.862	41.860
1.5	41.842	215.7989	-2	0.658	0.639	41.833	41.835	41.834
2.0	41.842	151.2396	0	0.651	0.682	41.856	41.861	41.859
2.0	41.842	119.0005	2	0.655	0.678	41.872	41.878	41.875
2.0	41.842	215.4297	-2	0.642	0.689	41.842	41.847	41.845

Table 3 : **Evaluation of the orders of kinetics of some computer generated DTA peaks.**

n	E_{in} (KJ/mole)	T_m (K)	r	R_{i1}	R_{i2}	n_1	n_1
1.0	41.842	151.4703	0	0.693	0.531	0.977	1.06
1.5	41.842	151.3532	0	0.668	0.631	1.45	1.49
2.0	41.842	151.2396	0	0.651	0.682	1.89	1.84

Table 4 : **Evaluation of the kinetic parameters of the experimental DTA curve of** $Ni(mpipz)_2(NCS)_2 2H_2O \rightarrow Ni(mpipz)_2(NCS)_2$ **recorded with a heating rate of** $5^0C/min$.

E_{BD} (KJ/mole)	E_p (KJ/mole)	n_p
144.13	145.10	1.42

Table 5 : **Evaluation of the temperature exponent of the experimental DTA curve of** $Ni(mpipz)_2(NCS)_2 2H_2O \rightarrow Ni(mpipz)_2(NCS)_2$ **recorded with a heating rates of** $5^0C/min$ and $10^0C/min$.

r_1	r_2	r_3	A_p (sec^{-1})
-7.23(-3)	+2.05(-2)	+6.68(-3)	7.83(16)

MINIMUM FILL-IN ON CACTUS GRAPHS

Anita Saha, Tapan K. Pal and Madhumangal Pal*
Department of Applied Mathematics with Oceanology and Computer Programmning
Vidyasagar University
Midnapore - 721 102, West Bengal, India.

August 17, 2001

Abstract :
The minimum fill-in problem is well known graph theoretic problem. This problem is NP-Complete for general graph as well as for some special class of graphs, such as co-bipartite graphs, bipartite graphs etc. The class of cactus graph is a subclass of plannar graphs. In this paper we present an O(n) time algorithm to solve minimum fill-in problem on cactus graphs.

Key words : Cactus graph, design and analysis of algorithm, minimum fill-in problem.

INTRODUCTION

The minimum fill-in problem is a well known graph theoretic problem. The minimum fill-in problem is NP-Complete for general graph and also for co-bipartite graphs [14] and on bipartite graphs [12]. But the polynomial time algorithms for chordal bipartite graphs [2], multitolerance graphs [8], d-trapeziod graphs [1], circle and circular-arc graphs [7], cographs [3], bipartite permutation graphs [11] are available for this problem.

The minimum fill-in problem has many similarities with the treewidth problem. Both problems ask for a chordal embedding of the graph. To the best of our knowledge we are not aware of any graph for which the two problems treewidth and minimum fill-in have different algorithmic complexity, although the solution for the two problems can be far apart.

The class of cactus graph is an important subclass of planar graphs. We present an algorithm to compute the minimum fill-in of cactus graph. The proposed algorithm compute a minimum triangulation of a certain convex polygon and has over all running time of $O(n)$. This shows that the cactus graph is an addition to classes of graphs for which the minimum fill-in problem can be solved in polynomial time.

*e-mail : madhumangal@lycos.com

PRELIMINARIES

Let $G = (V, E)$ be finite connected undirected simple graph of n vertices and m edges. Here V is the set of n vertices and E is the set of m edges. For a set $S \subseteq V$, the subgraphs of G induced by S is denoted by $G[S]$.

1. Preliminaries on triangulations

In this section we give some definitions and state some lemmas and theorems available in different literatures on triangulations and minimal separators.

Definition 1 *A cycle is a connected graph or subgraph in which every vertex is of degree two.*

Definition 2 *An edge joining two non-consecutive vertices of a cycle is called a chord.*

Definition 3 *A graph is said to be chordal if it does not contain a cordless cycle of length greater than 3. Alternately, a graph is called chordal if every cycle of length strictly greater than3 possesses a chord.*

Definition 4 *A triangulation of a graph G is a chordal graph H(G) with the same vertex set as G, such that G is a sub graph of H(G). A triangulation H(G) of a graph G is called a minimal triangulation of G, if no proper subgraph of H(G) is a triangulation of G.*

The following theorem is proved in [10].

Theorem 1 *Let H(G) be a triangulation of a graph G. Then H(G) is a minimal traingulation of G if and only if each edge $(u, v) \in E(H) - E(G)$ is the unique chord of a cycle of length 4 in H(G).*

Definition 5 *Let $G = (V, E)$ be a graph and u, v be two non-adjacent vertices of G. The set $S \subseteq V$ is an uv-separator if the removal of S separates u and v into two distinct connected components. If no proper subset of S is an uv-separator then S is a minimal uv-separator. A minimal separator is a set of vertices S for which there exist non-adjacent u and v such that S is a minimal uv-separator.*

A proof of the following well known lemma is given in [4].

Lemma 1 *Let S be a minimal uv-separator of the graph G = (V, E) and let C_u and C_v be the connected components of G[V - S] containing u and v respectively. Then every vertex of S has at least one neighbour in C_u and at least one neighbour in C_v.*

We denote by $\Delta(H)$ the set of all minimal separators of a graph H. In [6] the following characterization of minimal triangulation is given.

Theorem 2 *A triangulation H(G) of a graph G is minimal triangulation of G if and only if the following three conditions are satisfied.*
(i) If u and v are non-adjacent vertices of H(G) then every minimal uv-separator of H(G) is also a minimal uv-separator of G.
(ii) If S is a minimal separator of H(G) and C a connected component of H[V - S], then the vertex set of C also induces a connected component in G[V - S].
(iii) $H(G) = G_{\Delta(H)}$, where $G_{\Delta(H)}$ is the graph obtained from G by adding edges between every pair of vertices contained in the same set S for any $S \in \Delta(H)$.

In [5], Lipton and Tarjan have shown that for every planar graph we can find a separator of size $\sqrt{8.n}$. They presented an $O(n)$ time algorithm for finding separator. As cactus graph is a subgraph of planar graph, we have the following results.

Lemma 2 *A cactus graph on n verties has $O(\sqrt{n})$ minimal separator.*

Lemma 3 *There is an $O(n)$ time algorithm for computing the minimal separator of a cactus graph.*

Now we define the minimum fill-in problem as follows :

Definition 6 *The minimum fill-in problem is the problem of finding a triangulation H(G) of the given graph G = (V, E) with the least possible number of edges. The minimum fill-in of the graph G, denoted by mfiG, is the minimum number of edges to be added to make G a chordal.*

In other words, solving the minimum fill-in problem is equivalent to finding a triangulation $H(G)$ of the input graph G with smallest possible number of edges. Thus any perfect elimination ordering of $H(G)$ is a minimum elimination ordering of G.

2. Preliminaries on cactus graph

Here we give the necessary background material concerning cactus graph.

Definition 7 *A vertex v of V is called a cutvertex if removal of v and all edges incident on v disconnect the graph.*

Definition 8 *A connected graph without a cutvertex is called a non-separable graph.*

Definition 9 *A maximal non-separable subgraph of a graph is called a block of the graph.*

Definition 10 *A block which is a cycle is called a cyclic block.*

Definition 11 *A cactus graph is a connected graph in which every block is either an edge or a cycle.*

It follows from the definition of cactus graph that each block of it is either an edge or a cycle. If each cycle block is isomorphic to C_3 (cycle block of length 3) then the graph is said to be triangulated. Clearly, minimum fill-in of a triangulated graph is zero.

Figure 1 represented a cactus graph. The numbers within the circles represent the vertices.

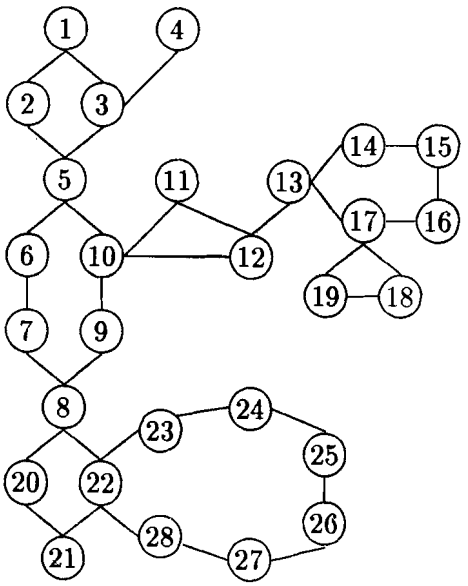

Figure 1 : A cactus graph

DETERMINATION OF BLOCKS

Blocks of any graph can be computed by applying DFS [9]. Let the set of all blocks obtained from the cactus graph $G = (V, E)$ be $B_1, B_2, ..., B_N$.

For the cactus graph of Figure 1 the blocks, thus obtained, are $B_1 = \{1, 2, 3, 5\}$, $B_2 = \{3, 4\}$, $B_3 = \{5, 6, 7, 8, 9, 10\}$, $B_4 = \{10, 11, 12\}$, $B_5 = \{12, 13\}$, $B_6 = \{13, 14, 15, 16, 17\}$, $B_7 = \{17, 18, 19\}$, $B_8 = \{8, 20, 21, 22\}$, $B_9 = \{22, 23, 24, 25, 26, 27, 28\}$.

It is proved in [13] that the number of edges of a cactus graph is of $O(n)$. The following lemma gives the maximum number of edges of a cactus graph.

Lemma 4 *The maximum number of edges in a cactus graph with n vertices is* [3(n-1)/2] *[13].*

We can compute all blocks of any graph using DFS [9]. Therefore, using same algorithm we can compute all blocks of a cactus graph. Again the blocks of any graph can be computed in $O(|V| + |E|)$ time [9]. As for any cactus graph, $|E|$ is of $O(n)$ (Lemma 4), the time complexity to compute all blocks of a cactus graph is given below.

Lemma 5 *All block of any cactus graph can be computed in $O(n)$ time.*

The blocks of any cactus graph are either edge or C_3 or C_{2k+1} or C_{2k} $(k \geq 2)$.

Definition 12 *The triangle of a cactus graph is C_3, i.e., the cycle-block of length 3.*

Definition 13 *The blocks of types C_{2k} or C_{2k+1} $(k \geq 2)$ are called polygons.*

Definition 14 *The length of a cycle is the number of edges (or vertices) in the cycle.*

Definition 15 *The number of edges (or, vertices) of a polygon is called the length or cardinality of the polygon.*

The convex polygons for the cactus graph of Figure 1 are B_1, B_3, B_6, B_8, and B_9 and the triangles are B_4 and B_7.

If the cactus graph G has no polygons then G is already triangulated and hence, in this case minimum fill-in is 0.

TRIANGULATION OF A POLYGON

As all cycles C_n, $n > 2$, can be represented in a plane as a convex polygon, we refer all polygons as convex polygons.

Without loss of generality let the vertices of a convex polygon P be $Y = \{v_1, v_2, ..., v_k\}$ where k is the length of the polygon, and we denote $P(Y)$ as a convex polygon with vertex set Y.

We assume that $v_1, v_2, ..., v_k$ are in a cycle order. That is, $(v_1, v_2), (v_2, v_3), ...(v_{k-1}, v_k)$ and (v_k, v_1) are the edges of G. Let $H(P)$ be the triangulation of P. The triangulation of a polygon can be obtained in many different ways. One of the systematic and simple way is

"join v_1 with $v_i, i = 3, 4, ..., k - 1$".

It may be noted that all the new edges are non-crossing.

The triangulation technique is illustrated in Figure 2.

By the construction procedure of $H(P)$ it is obvious that the number of edges of $H(P)$ is $|P| + (|P| - 3)$ or, $2|P| - 3$. The number of triangle of $H(P)$ is $|P| - 2$.

Lemma 6 *Let P be a convex polygon with k vertices. A triangulation of P is a set of k - 3 non-crossing edges in P that divide the interior of P into k - 2 triangles.*

Lemma 7 *The subgraph H(P) is chordal and therefore a triangulation of P.*

It may be noted that P is a spanning subgraph or exterior of $H(P)$.

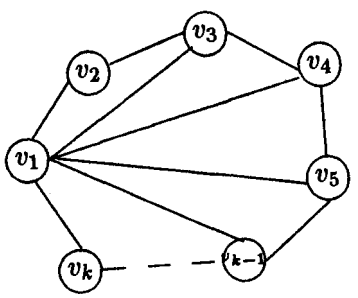

Figure 2 : Triangulation of a convex polygon

ALGORITHM AND ITS COMPLEXITY

In this section we describe simple linear time algorithm to find the minimum fill-in of cactus graph. The major steps to compute minimum fill-in of cactus graph are presented below.

Algorithm MINIMUM-FILL-IN
Input : A cactus graph G.
Output : A triangulation $H(G)$ and $mfi(G)$.

Step 1 : Compute all blocks of G.
Step 2 : Identify all polygons among blocks obtained from Step 1. Let the polygons be $B_1, B_2, \ldots, B_{N'}$, where N' represents the total number of polygons.
Step 3 : If N' is equal to zero then set $mfi(G) = 0$ and stop.
Step 4 : Compute $H(B_i)$ for all polygons B_i, $1 \leq i \leq N'$.
Step 5 : Compute $\Sigma_{i=1}^{N'} (|B|_i - 3)$ and set it to $mfi(G)$.

end MINIMUM-FILL-IN

The time complexity of the above algorithm is given in the following theorem.

Theorem 3 *The minimum fill-in problem on cactus graphs with n vertices can be computed in $O(n)$ time.*

Proof. The blocks of any graph can be computed in $O(|V| + |E|)$ time [9]. For cactus graph, $|E|$ is of $O(n)$ (Lemma 4). Identification of polygons among blocks can be done in $O(n)$ time. Step 4 of Algorithm MINIMUM-FILL-IN takes only $O(\Sigma_{i=1}^{N'}(|B_i| - 3))$, i.e., $O(n)$ time, where N' represents the total number of polygons. Hence, the overall time complexity is of $O(n)$.

The graph $H(G)$ of the graph G of Figure 1 is shown in Figure 3.
Since $\Sigma_{i=1}^{N'}(|B_i| - 3)$ is of $O(n)$, we have the following results.

Result 1 The number of vertices and edges of $H(G)$ (triangulation of G) are n and $O(n)$ respectively.

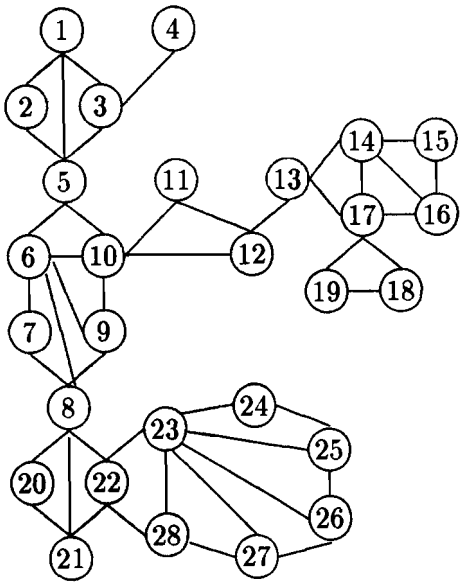

Figure 3 : The triangulation $H(G)$ of the graph G of Figure 1.

Result 2 The graph $H(G)$ is chordal as well as planar.

REFERENCES

[1] H. Bodlaender, T. Kloks, D. Kratsch and H. Miiller, Treewidth and minimum fill-in on *d*-trapezoid graphs, Technical Report UU-CS-1995-34, Utrecht University, The Netherlands.

[2] M.-S. Chang, Algorithms for minimum matching and minimum fill-in on chordal bipartite graphs, in *"Proceedings of ISAAC' 96", Lecture Notes in Computer Science,* Vol. 1178, 146-155, Springer-Verlag, New York, 1996.

[3] D. G. Corneil, Y. Perl and L. K. Stewart, Cographs : Recognitions and algorithms, *Congr. Numer.*, 43 (1984) 249-258.

[4] M. C. Golumbic, *Algorithmic Graph Theory and Prefect Graphs*, Academic Press, New York, 1980.

[5] R. J. Lipton and R. E. Tarjan, A separator theorem for planar graphs, *SIAM J. Appl. Math.*, 36 (1979) 177-189.

[6] T. Kloks, D. Kratsch and H. Miiller, Approximation the bandwidth of AT-free graphs, in *"Proceeding of ESA 1995", Lecture Notes in Computer Science,* Vol. 979, 434-447, Springer-Verlag, New York, 1995.

[7] T. Kloks, D. Kratsch and C. K. Wong, Minimum fill-in on circle and circular-arc graphs, *J. Algorithms*, 28 (1998) 272-289.

[8] A. Parra, Triangulating multitolerance graphs, Technical Report 392/1994, Technische Universität Berlin, Germany.

[9] E. M. Reingold, J. Nivergent and N. Deo, *Combinatorial Algorithms : Theory and Practice*, Prentice Hall, Inc., Englewood Chiffs, New Jersey, 1977.

[10] D. J. Rose, R. E. Tarjan and G. S. Lueker, Algorithmic aspects of vertex elimination on graph, *SIAM J. Comput.*, 5 (1976) 266-283.

[11] J. Spinrad, A. Brandstädt and L. Kstewart, Bipartite permutation graphs, *Discrete Appl. Math.*, 18 (1987) 279 - 292.

[12] R. E. Tarjan, Decomposition by clique separators, *Discrete Mathematics*, 55(1985) 221 - 232.

[13] D. B. West, *Introduction to Graph Theory*, Prentice - Hall of India Pvt. Ltd., New Delhi, 1999.

[14] M. Yannakakis, Computing the minimum fill-in is NP-Complete, *SIAM J. Algebraic Discrete Methods*, 2 (1981) 77 - 79.

HALL EFFECTS ON UNSTEADY COUETTE FLOW UNDER BOUNDARY LAYER APPROXIMATIONS

R. N. Jana and A. K. Kanch
Department of Applied Mathematics
Vidyasagar University
Midnapur - 721 102, West Bengal, India.

Abstract :

The effects of Hall current on the unsteady hydromagnetic Couette flow between two infinite horizontal parallel plates is considered. An exact solution of the governing equations has been obtained by using Laplace transform technique. It is found that for large time the transient effects die out exponentially and the ultimate steady flow consists of Stokes-Hartmann boundary layers near the plates. The thicknesses of these boundary layers increase with increase in Hall parameter.

INTRODUCTION

Hall effects on the steady hydromagnetic flow between two parallel plates have been studied by Sato [1], Sherman and Sutton [2], Yamanishi [3]. On the other hand the Couette flow of a conducting gas between two parallel plates in the presence of transverse magnetic field have been investigated by Gubanov and Lunkin [4] and Pelelier and Wijngaarden [5]. The effects of Hall current on the oscillatory magnetohydrodynamic flow past a flat plate has been studied by Datta and Jana [6].

In the present paper, we have studied the effects of Hall current on the unsteady hydromagnetic Couette flow between two infinite long horizontal parallel plates under boundary layer approximations. At time $t > 0$, the upper plate excecute non-torsional oscillation with given frequency and the lower plate is at rest. An exact solution is obtained by using Laplace transform technique. It is shown that the transient effects die out exponentially as $t \to \infty$ and the ultimate steady flow consists of Stokes-Hartmann boundary layers near the plate. The thicknesses of these boundary layers increases with increase in Hall parameter m. We have also examined several limiting cases of interest.

MATHEMATICAL FORMULATION AND ITS SOLUTION

Consider the unsteady two-dimensional viscous incompressible electrically conducting fluid bounded by two infinite long horizontal parallel plates at $y = 0$ and $y = d$. At time $t \leq 0$, the plates and the fluid are at rest but at time $t > 0$, the plate at $y = d$ starts to oscillate non-torsionally in its own plane. The x - axis in the direction of the flow and z - axis normal to the xy - plane. A uniform transverse magnetic field H_0 is applied parallel to y - axis. Since the plates are infinitely long x and z directions, all physical quantities, except pressure, will be function of y and t only. As Hall currents interacts with the magnetic field to generate a transverse motion of the field, the flow field can be taken as (u', 0, w').

We shall assume that the induced magnetic field produced by the motion of the conducting fluid is negligible so that $H \equiv (0, H_0, 0)$. We also assume that electric field $\vec{E} = 0$, [see Mayer [7]. Neglecting ion-slip and thermoelectric effects, the generalized Ohm's law for partially ionized gas is, Sato [1],

$$\vec{j} + \frac{\omega_e \tau_e}{H_0}(\vec{j} \times \vec{H}) = \sigma \mu_e \vec{q} \times \vec{H}, \tag{1}$$

where $\vec{q}$, $\vec{j}$, σ, μ_e, ω_e and τ_e are respectively, the fluid velocity vector, the current density vector, the conductivity of the fluid, the magnetic permeability, the cyclotron frequency and electron collision time.

Using (1) , the Navier - stokes equations of motion for a conducting fluid are

$$\frac{\partial u'}{\partial t} = -\frac{1}{\rho}\frac{\partial p}{\partial x} + \nu \frac{\partial^2 u'}{\partial y^2} - \frac{\sigma \mu_e^2 H_0^2 (u' + m w')}{\rho (1 + m^2)}, \tag{2}$$

$$0 = -\frac{1}{\rho}\frac{\partial p}{\partial x}, \tag{3}$$

$$\frac{\partial w'}{\partial t} = -\frac{1}{\rho}\frac{\partial p}{\partial z} + \nu \frac{\partial^2 w'}{\partial y^2} - \frac{\sigma \mu_e^2 H_0^2 (m u' - w')}{\rho (1 + m^2)}, \tag{4}$$

where ρ, ν, p and $m(= \omega_e \tau_e)$ are respectively the fluid density, the kinematic viscosity, the

fluid pressure and the Hall parameter.

The initial and boundary conditions are

$$u' = w' = 0 \text{ for } t \le 0 \text{ and } 0 \le y \le d, \tag{5}$$

$$u' = 0 = w' \text{ at } y = 0 \text{ for } t > 0$$

and

$$u' = U(t), w' = 0 \text{ at } y = d \text{ for } t > 0. \tag{6}$$

Under usual boundary layer approximations, equations (2) and (4) become

$$\frac{\partial u'}{\partial t} = \frac{\partial U}{\partial t} + \nu \frac{\partial^2 u'}{\partial y^2} - \frac{\sigma \mu_e^2 H_0^2 [u' - U + m w']}{\rho(1 + m^2)}, \tag{7}$$

$$\frac{\partial w'}{\partial t} = \nu \frac{\partial^2 w'}{\partial y^2} + \frac{\sigma \mu_e^2 H_0^2 [m(u' - U) - w']}{\rho(1 + m^2)}. \tag{8}$$

Introducting non-demensional variables

$$\eta = \frac{y}{d}, u = \frac{u'}{U_0}, w = \frac{w'}{U_0}, U = U_0 f(\tau), \tau = \frac{\nu t}{d^2}, M^2 = \frac{\sigma \mu_e^2 H_0^2 d^2}{\rho \nu}, \tag{9}$$

equations (7) and (8) become

$$\frac{\partial u}{\partial \tau} = \frac{\partial f}{\partial \tau} + \frac{\partial^2 u}{\partial \eta^2} - \frac{M^2 [u - f + m w]}{1 + m^2}, \tag{10}$$

$$\frac{\partial w}{\partial \tau} = \frac{\partial^2 w}{\partial \eta^2} + \frac{M^2 [m(u - f) - w]}{1 + m^2}. \tag{11}$$

Equations (10) and (11) can be combined as

$$\frac{\partial q}{\partial \tau} = \frac{\partial f}{\partial \tau} + \frac{\partial^2 q}{\partial \eta^2} - \frac{M^2 (1 + im)(q - f)}{1 + m^2} . \tag{12}$$

where

$$q = u + iw . \tag{13}$$

Using (9) and (13), the initial and the boundary conditions given by (5) and (6) become

$$q = 0 \text{ for } \tau \leq 0 \text{ and } 0 \leq \eta \leq 1 \tag{14}$$

and

$$q = 0 \text{ at } \eta = 0 \text{ and } q = f(\tau) \text{ at } \eta = 1 \text{ for } \tau > 0. \tag{15}$$

The non-dimensional oscillatory velocity $f(\tau)$ of the plate is assumed to be

$$f(\tau) = 1 + [ae^{i\omega\tau} + be^{-i\omega\tau}], \tag{16}$$

where a and b are complex constants and $w = \omega^* v / d^2$, ω^* being the frequency of the oscillations.

Using Laplace transform and the conditions

$$q^* (o, s) = o, \; q^* (\infty , p) = \frac{1}{s} + \frac{a}{s - i\omega} + \frac{b}{s + i\omega} , \tag{17}$$

(which follow from equations (15) and (16)), equations (14) and (12) give

$$q^* (\eta , s) = [\frac{1}{s} + \frac{a}{s - i\omega} + \frac{b}{s + i\omega}] [1 - \frac{\sinh \{s + \frac{M^2(1 + im)}{1 + m^2}\}^{\frac{1}{2}} (1 - \eta)}{\sinh \{s + \frac{M^2(1 + im)}{1 + m^2}\}^{\frac{1}{2}}}], \tag{18}$$

where q* (η , s) is the Laplace transform of $q(\eta , \tau)$.

Taking inverse Laplace transform of equation (18), we get

$$q(\eta, \tau) = [1 - \frac{\sinh(\alpha + i\beta)(1 - \eta)}{\sinh(\alpha + i\beta)}]$$

$$+ ae^{i\omega\tau}[1 - \frac{\sinh(\alpha_1 + i\beta_1)(1 - \eta)}{\sinh(\alpha_1 + i\beta_1)}]$$

$$+ be^{-i\omega\tau}[1 - \frac{\sinh(\alpha_2 \pm i\beta_2)(1 - \eta)}{\sinh(\alpha_2 \pm i\beta_2)}]$$

$$- 2\pi \sum_{i=1}^{\infty} [\frac{1}{s_1} + \frac{a}{s_1 - i\omega} + \frac{b}{s_1 + i\omega}] \sin(n\pi\eta) e^{s_1\tau}, \qquad (19)$$

where positive sign for $\omega < mM^2/(1 + m^2)$ and negative sign for $\omega > mM^2/(1 + m^2)$ and

$$\alpha, \beta = \frac{1}{\sqrt{2}} [\frac{M^2}{1 + m^2}]^{1/2} [(1 + m^2)]^{1/2} \pm 1]^{1/2},$$

$$\alpha_1, \beta_1 = \frac{1}{\sqrt{2}} [\{(\frac{M^2}{1 + m^2})^2 + (\omega + \frac{mM^2}{1 + m^2})^2\}^{1/2} \pm \frac{M^2}{1 + m^2}]^{1/2}, \qquad (20)$$

$$\alpha_2, \beta_2 = \frac{1}{\sqrt{2}} [\{(\frac{M^2}{1 + m^2})^2 + (\omega - \frac{mM^2}{1 + m^2})^2\}^{1/2} \pm \frac{M^2}{1 + m^2}]^{1/2},$$

$$s_1 = - [n^2\pi^2 + \frac{M^2(1 + im)}{1 + m^2}].$$

The equation (19) describes the fluid velocity in the general case. Many particular results emerge easily from the solution which are given below.

THE STEADY STATE SOLUTION

The principal feature of the solution is that first three terms of (19) represent the steady state components and remaining infinite series combined, together constitute the transient solution. In the limit $t \to \infty$, the transient part of the solution (19) decays very quickly and the steady state is reached and the fluid velocity is given by

$$q(\eta, \tau) = [1 - \frac{\sinh(\alpha + i\beta)(1 - \eta)}{\sinh(\alpha + i\beta)}]$$

$$+ ae^{i\omega\tau}[1 - \frac{\sinh(\alpha_1 + i\beta_1)(1 - \eta)}{\sinh(\alpha_1 + i\beta_1)}]$$

$$+ be^{-i\omega\tau}[1 - \frac{\sinh(\alpha_2 \pm i\beta_2)(1 - \eta)}{\sinh(\alpha_2 \pm i\beta_2)}]. \qquad (21)$$

The steady state solution consists of multiple boundary layers of thicknesses $\frac{1}{\alpha}, \frac{1}{\alpha_1}$, and $\frac{1}{\alpha_2}$ where α, α_1 and α_2 are given by (20). It is seen that α, α_1 and α_2 all decrease with increase in Hall parameter m. Hence, we conclude that the boundary layers thicknesses increase with the increase in Hall parameter. If $m = 0$ and $a = b = \frac{\epsilon}{2}$, then $w = 0$ and u coincides with the result of Vajravelu [8]

In the limit $d \to \infty$, the steady state solution for the velocity field is given by

$$u' + iw' = U_0\{1 - e^{-(\alpha^* + i\beta^*)\frac{z}{\sqrt{2}v}}$$

$$+ ae^{i\omega\tau}[1 - e^{-(\alpha_1^* + i\beta_1^*)\frac{z}{\sqrt{2}v}}]$$

$$+ be^{-i\omega\tau}[1 - e^{-(\alpha_2^* + i\beta_2^*)\frac{z}{\sqrt{2}v}}]\}, \qquad (22)$$

where

$$\alpha^*, \beta^* = (\frac{\sigma}{\rho})^{1/2} \frac{\mu_e H_0}{\sqrt{(1 + m^2)}} [(1 + m^2)^{1/2} \pm 1]^{1/2},$$

$$\alpha_1^*, \beta_1^* = [\{(\frac{\sigma\mu_e^2 H_0^2}{\rho(1 + m^2)})^2 + (\omega^* + \frac{m\sigma\mu_e^2 H_0^2}{\rho(1 + m^2)})^2\}^{1/2} \pm \frac{\sigma\mu_e^2 H_0^2}{\rho(1 + m^2)}]^{1/2}, \qquad (23)$$

$$\alpha_2^*, \beta_2^* = [\{(\frac{\sigma\mu_e^2 H_0^2}{\rho(1+m^2)})^2 + (\omega^* - \frac{m\sigma\mu_e^2 H_0^2}{\rho(1+m^2)})^2\}^{1/2} \pm \frac{\sigma\mu_e^2 H_0^2}{\rho(1+m^2)}]^{1/2},$$

When $a = b = \frac{\epsilon}{2}$, then, on separating real and imaginary parts, we get

$$u'(\eta, \tau) = U_0\{1 - e^{-\alpha^* \frac{z}{\sqrt{2v}}} \cos(\frac{\beta^* z}{\sqrt{2v}}) + \frac{\epsilon}{2}[2\cos\omega^* t - e^{-\alpha_1^* \frac{z}{\sqrt{2v}}} \cos(\omega^* t - \beta_1^* \frac{z}{\sqrt{2v}}) - e^{-\alpha_2^* \frac{z}{\sqrt{2v}}} \cos(\omega^* t \pm \beta_2^* \frac{z}{\sqrt{2v}})\}, \quad (24)$$

$$w'(\eta, \tau) = U_0\{e^{-\alpha^* \frac{z}{\sqrt{2v}}} \sin(\frac{\beta^* z}{\sqrt{2v}}) + \frac{\epsilon}{2}[e^{-\alpha_2^* \frac{z}{\sqrt{2v}}} \sin(\omega^* t \pm \beta_2^* \frac{z}{\sqrt{2v}}) - e^{-\alpha_1^* \frac{z}{\sqrt{2v}}} \sin(\omega^* t - \beta_1^* \frac{z}{\sqrt{2v}})]\}, \quad (25)$$

where α^*, β^*, α_1^*, β_1^*, α_2^*, β_2^*, are given by (23). The above equations (24) and (25) show that in the limit $d \to \infty$, the steady state solution for the fluid velocities corresponds to single plate problem when free - stream oscillates in its own plane with velocity $U_0(1 + \epsilon\cos\omega^* t)$ about a constant mean velocity U_0.

The unsteady part of the velocity fields consists of two parts one oscillating with amplitude $\frac{\epsilon}{2}\exp(-\alpha_1^* \frac{z}{\sqrt{2v}})$ and the other $\frac{\epsilon}{2}\exp(-\alpha_2^* \frac{z}{\sqrt{2v}})$. The layer corresponding to the amplitude $\frac{\epsilon}{2}\exp(-\alpha_1^* \frac{z}{\sqrt{2v}})$ at a distance z from the plate oscillates with a phase lag of $\beta_1^* \frac{z}{\sqrt{2v}}$ while the layer corresponding to the amplitude $\frac{\epsilon}{2}\exp(-\alpha_2^* \frac{z}{\sqrt{2v}})$ oscillates with a phase advance of $\beta_2^* \frac{z}{\sqrt{2v}}$ for $\omega < \frac{mM^2}{1+m^2}$ and phase lag of $\beta_2^* \frac{z}{\sqrt{2v}}$ for $\omega > \frac{mM^2}{1+m^2}$. The depth of penetration or wave length of the two layers are $\frac{2\sqrt{2}v\pi}{\beta_1^*}$ and $\frac{2\sqrt{2}v\pi}{\beta_2^*}$ respectively.

If $\epsilon = 0$, then the equations (24) and (25) reduce to

$$u_1'(\eta, \tau) = U_0\{1 - e^{\alpha^* \frac{z}{\sqrt{2v}}} \cos(\beta^* \frac{z}{\sqrt{2v}})\}, \quad (26)$$

$$w_1'(\eta, \tau) = U_0\{e^{-\alpha^* \frac{z}{\sqrt{2\nu}}} \sin(\beta^* \frac{z}{\sqrt{2\nu}})\}, \quad (27)$$

These are the velocity components corresponding to the flow past a flat plate when the free-stream velocity is uniform. This result agrees with the equation (43) of Datta and Jana [7].

SOLUTION FOR NON-OSCILLATING CASE

In this case, the velocity field is obtained from (19) by substituting $\omega = 0$ as

$$q = (1 + a + b)\{[1 - \frac{\sinh(\alpha + i\beta)(1 - \eta)}{\sinh(\alpha + i\beta)}] - 2\pi \sum_{n=1}^{\infty} \frac{n \sin n\pi\eta}{s_1} e^{s_1 \tau}\}, \quad (28)$$

where s_1 is given by (20). The transient term in (28) decays to zero as $t \to \infty$. Thus the steady state solution is established in the limit and represents the Stocks-Hartmann boundary layer. The thickness of this boundary layer is of order $\frac{1}{\alpha}$, where α is given by (20). The time required for the transient effects to decay of the order

$$[n^2\pi^2 + \frac{M^2}{1 + m^2}]^{-1}$$

which is modified due to the presence of Hall current and always greater than the magnetic diffusion time $[n^2\pi^2 + M^2]^{-1}$.

RESULTS AND DISCUSSION

In order to study the effects of Hall current on the distribution of velocity fields, we plotted u and w against η for $a = b = \frac{1}{2}$, $\omega\tau = \frac{\pi}{2}$, $M^2 = 10$ in figures -1 and 2 for various values of Hall parameter m and frequency parameter ω. It is seen from fig.1 that the primary velocity u decreases whereas secondary velocity w increases in Hall parameter m. For fixed value of m, figure -2 shows that, when ω is small then the primary velocity decreases with increases in ω. On the other hand, for large values ω, it decreases near the stationary plate $\eta = 0$ and increases near the oscillating plate $\eta = 1$ when m is fixed. It also shows that there is an incipent reverse flow near the stationary plate $\eta = 0$ for large values of ω. Further it is seen that the secondary velocity increases with increase in ω when m is fixed.

The shear stresses due to the primary and the secondary flow at the stationary plate $\eta = 0$ is given by

$$\tau_x + i\tau_y = \frac{\partial q}{\partial \eta}]_{\eta=0} = \frac{(\alpha + i\beta)\cosh(\alpha + i\beta)}{\sinh(\alpha + i\beta)}$$

$$+ ae^{i\omega\tau}\frac{(\alpha_1 + i\beta_1)\cosh(\alpha_1 + i\beta_1)}{\sinh(\alpha_1 + i\beta_1)}$$

$$+ be^{-i\omega\tau}\frac{(\alpha_2 \pm i\beta_2)\cosh(\alpha_2 \pm i\beta_2)}{\sinh(\alpha_2 \pm i\beta_2)}$$

$$- 2\pi^2 \sum_{n=1}^{\infty} n^2(-1)^n[\frac{1}{s_1} + \frac{a}{s_1 - i\omega} + \frac{b}{s_1 + i\omega} +]e^{s_1\tau} \ ,$$

from which on separating real and imaginary parts, one can easily obtain τ_x and τ_y.

The values of τ_x and τ_y at the plate $\eta = 0$ have been plotted against m for $a = b = \frac{1}{2}$, $M^2 = 10$ in figures -3 and 4 for different values of ω and $\omega\tau$. It is seen from figure 3 that for fixed ω, the shear - stress τ_x due to the primary flow decreases with increase in either m or $\omega\tau$, while for fixed values of m and $\omega\tau$, it increases with increase in frequency ω. It is observed from figure -4 that for fixed values of $\omega\tau$, the shear stress τ_y due to the secondary flow increases with increase in either m or ω. It is also observed that for fixed values of ω, with increase in $\omega\tau$, it decrease for small values of m while it increases for large values of m when $\omega\tau < 45^0$ and the results is reversed when $\omega\tau > 45^0$.

REFERENCES

[1] Sato H, J. Phys. Soc. of Japan 16 (1961) 1427.

[2] Sherman A and Sutton G W, Engineering Magnetohydrodynamics, New York, Mc-Graw Hill book company, 1995.

[3] Yamanishi T, Preprint, 17 Annual meeting, Phys. Soc. of Japan, 5 (1962)29.

[4] Gubanov A J and Lunkin P T, Sov. Phys. - Tech. Phys., 5 (1961) 984.

[5] Paletier L A and Wijngaarden L Van, Appl. Sci Res., 9*B* (1961) 141.

[6] Datta N and Jana R N, J. Phys. Soc. Japan, 40 (1976) 1469.

[7] Vajravelu K, Trans. of ASME J. of Appl. Mech., 55 (1988) 981.

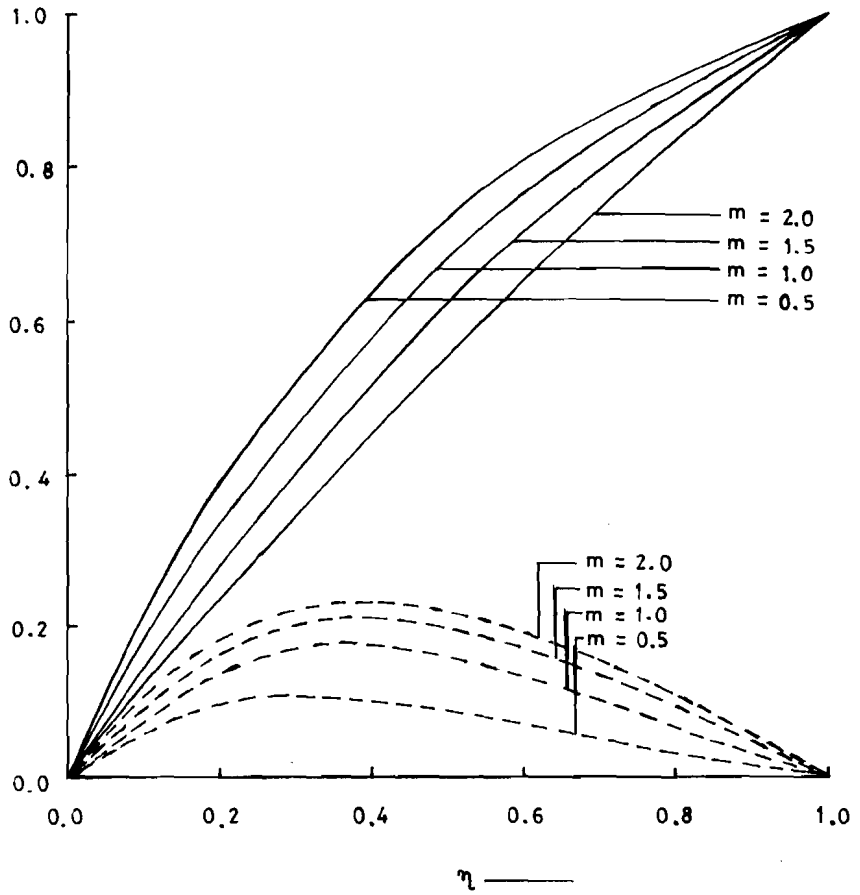

Fig.1 Velocity components ——— u and - - - - W for $\omega = 3.0, M^2 = 10.0$ $\tau = 0.5$, $a = b = 1/2$, $\omega\tau = 90^\circ$

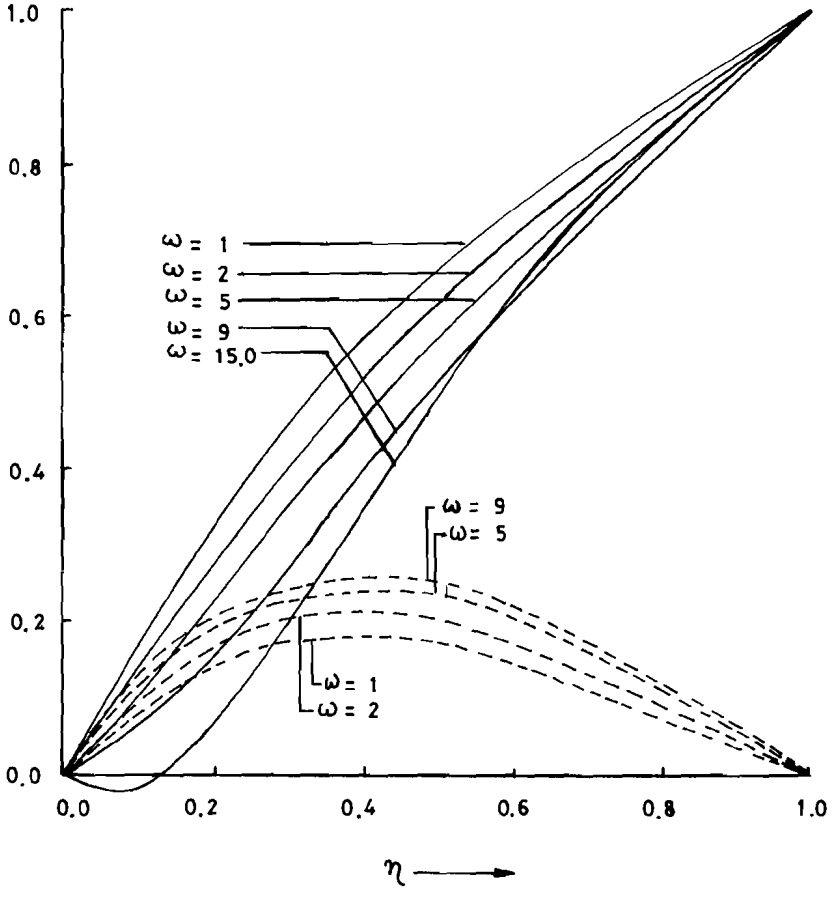

Fig. 2 Velocity components ——— u and -------W for $m = 1.5$, $M^2 = 10.0$
$\tau = 0.5$, $\omega\tau = 90^\circ$, $a = b = 1/2$

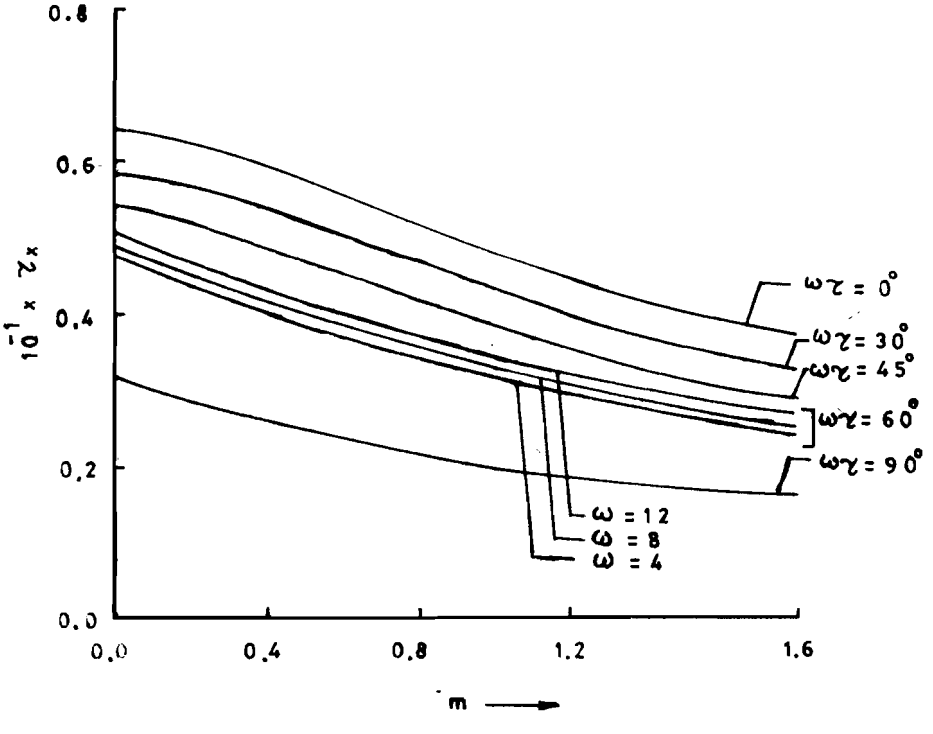

Fig. 3 Shear-stress due to primary velocity, for $M^2 = 10.0$ $\tau = 0.2$ $a = b = 1/2$

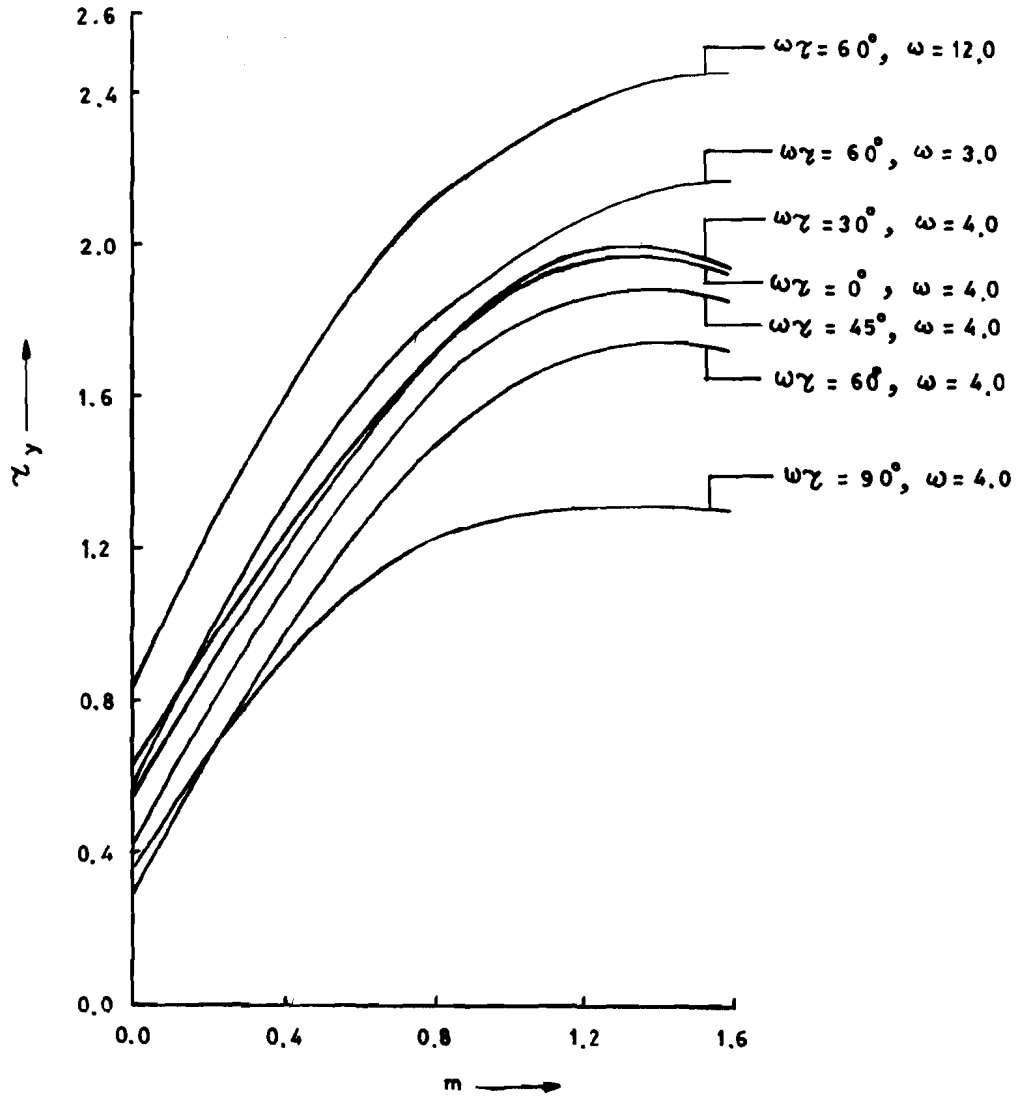

Fig. 4 Shear-stress due to secondary velocity for $M^2 = 10.0$ $\tau = 0.2$ $a = b = 1/2$

INTUITIONISTIC FUZZY DETERMINANT

Madhumangal Pal
Department of Applied Mathematics with Oceanology and Computer Programmning
Vidyasagar University
Midnapore - 721 102, West Bengal, India.

August 16, 2001

Abstract :
In this paper, intuitionistic fuzzy determinant (IFD) is introduced. Some common properties of IFD are also presented. Null IFD, triangular IFD, unit IFD and transpose of an IFD are also defined.

Key words : Intuitionistic fuzzy set, Intuitionistic fuzzy matrix, Inuitionistic fuzzy determinant.

INTRODUCTION

The fuzzy determinant is introduced first time by Kim [2, 3] and several properties are studied in [1]. In this paper, intuitionistic fuzzy determinant (IFD) is introduced and some properties are presented.

Throughout this paper, let F be a closed unit interval, i.e., $F = [0, 1]$ and

$$< F > = \{< a,b > : 0 \le a + b \le 1, a, b \in F\}.$$

Let M be the set of all square matrices of order $n \times n$ whose elements belong to a field X. X is said to be the field of scalars.

Definition 1 *A square fuzzy matrix (FM) A of order* $n \times n$ *is defined as* $A = [< a_{ij} , a_{ij\mu} >]_{n \times n}$ *where* $a_{ij\mu}$ *is the membership value of the element* a_{ij} *in A and* $a_{ij\mu} \in F$.

For simplicity we write A as $A = [a_{ij\mu}]_{n \times n}$.

Definition 2 *A square intuitionistic fuzzy matrix (IFM) A of order* $n \times n$ *is defined as*

$$A = [< x_{ij} , a_{ij\mu} , a_{ij\nu} >]_{n \times n}$$

where $a_{ij\mu}$ *and* $a_{ij\nu}$ *are called membership and non-membership values of* x_{ij} *in A, with the condition* $0 \le a_{ij\mu} + a_{ij\nu} \le 1$. *For simplicity we write* $A = [< x_{ij} , a_{ij} >]_{n \times n}$ *or,* $[a_{ij}]_{n \times n}$, *where* $a_{ij} = < a_{ij\mu} , a_{ij\nu} >$.

In arithmetic operations (such as addition, multiplication etc.) only the values of

$a_{ij\mu}$ and $a_{ij\nu}$ are needed so from here we only consider the values of $a_{ij} = < a_{ij\mu}, a_{ij\nu} >$. Note that all elements of an IFM are the members of $< F >$.

PRELIMINARIES

1. Fuzzy determinant

A mapping $f : M \to F$ which assigns to each fuzzy matrix A in M a scalar $c \in F$ is to be a scalar function on M and this scalar function is called determinant function on M.

Definition 3 *A fuzzy determinant (FD) function $f : M \to F$ is a scalar function on the set M of all $n \times n$ fuzzy matrices over the field F such that if $A \in M$ then $f(A)$ or $|A|$ or det (A) is a scalar belongs to F and is given by*

$$|A| = \sum_{\sigma \in S_n} a_{1\sigma(1)\mu} a_{2\sigma(2)\mu} \ldots a_{n\sigma(n)\mu} = \sum_{\sigma \in S_n} \prod_{i=1}^{n} a_{i\sigma(i)\mu}$$

where S_n denotes the symmetric group of all permutations of the symbols $\{1, 2, \ldots, n\}$. The summation Σ_σ is said to be the expansion of $|A|$.

Definition 4 *The addition and multiplication between two members of F are defined as follows :*

$$a_{ij\mu} + b_{ij\mu} = max\{a_{ij\mu}, b_{ij\mu}\}, \; a_{ij\mu} . b_{ij\mu} = min\{a_{ij\mu}, b_{ij\mu}\}.$$

EXAMPLE 1 : Let

$$A = \begin{bmatrix} 0.2 & 0.5 & 0.1 \\ 0.3 & 0.4 & 0.2 \\ 0.0 & 1.0 & 0.3 \end{bmatrix}$$

be a FM. We calculate |A| as follows :

$$|A| = 0.2 \begin{vmatrix} 0.4 & 0.2 \\ 1.0 & 0.3 \end{vmatrix} + 0.5 \begin{vmatrix} 0.3 & 0.2 \\ 0.0 & 0.3 \end{vmatrix} + 0.1 \begin{vmatrix} 0.3 & 0.4 \\ 0.0 & 1.0 \end{vmatrix}$$

$= 0.2(0.3 + 0.2) + 0.5(0.3 + 0.0) + 0.1(0.3 + 0.0) = 0.2(0.3) + 0.5(0.3) + 0.1(0.3)$
$= 0.2 + 0.3 + 0.1 = 0.3$

Several properties on FD are presented in [1, 2]. Two such important properties are stated below.

Theorem 1 *[1] Let A be a square FM of order n × n.*
(i) If A contains a zero row (column) then |A| = 0.
(ii) If A is triangular (a FM is triangular if $a_{ij} = 0$, for either i > j or i < j) then $|A| = \Pi^{n}_{i=1} a_{ii\mu}$.

2. Intuitionistic fuzzy determinant

Definition 5 *An intuitionistic fuzzy determinant (IFD) function $f_I : M \to < F >$ is a function on the set M (of IFM) of all n × n intuitionistic fuzzy matrices over < F > such that if $A \in M$ then f (A) or |A| or det (A) belongs to < F > and is given by*

$$|A| = \sum_{\sigma \in S_n} \prod_{i=1}^{n} a_{i\sigma(i)},$$

where $a_{i\sigma(i)} = < a_{i\sigma(i)\mu}, a_{i\sigma(i)\nu} >$ *and S_n denotes the symmetric group of all permutations of the symbols* { 1,2, ..., n}.

Definition 6 *The addition and multiplication between two elements a_{ij} and b_{ij} of < F > are defined as followes :*

$$a_{ij} + b_{ij} = < a_{ij\mu}, a_{ij\nu} > + < b_{ij\mu}, b_{ij\nu} > = < max(a_{ij\mu}, b_{ij\mu}),\ min\ (a_{ij\nu}, b_{ij\nu}) >$$
$$a_{ij} . b_{ij} = < a_{ij\mu}, a_{ij\nu} > . < b_{ij\mu}, b_{ij\nu} > = < min(a_{ij\mu}, b_{ij\mu}),\ max\ (a_{ij\nu}, b_{ij\nu}) >$$

It may be noted that the value of an IFD belongs to < F >.
EXAMPLE 2 : Let

$$A = \begin{bmatrix} < 0.5, 0.4 > & < 0.2, 0.7 > & < 0.1, 0.7 > \\ < 0.6, 0.2 > & < 1.0, 0.0 > & < 0.2, 0.5 > \\ < 0.8, 0.2 > & < 0.0, 1.0 > & < 0.5, 0.5 > \end{bmatrix}$$

be an IFM.
Then

$$|A| = < 0.5, 0.4 > \begin{vmatrix} < 1.0, 0.0 > & < 0.2, 0.5 > \\ < 0.0, 1.0 > & < 0.5, 0.5 > \end{vmatrix} + < 0.2, 0.7 > \begin{vmatrix} < 0.6, 0.2 > & < 0.2, 0.5 > \\ < 0.8, 0.2 > & < 0.5, 0.5 > \end{vmatrix}$$

$$+ < 0.1, 0.7 > \begin{vmatrix} < 0.6, 0.2 > & < 1.0, 0.0 > \\ < 0.8, 0.2 > & < 0.0, 1.0 > \end{vmatrix}$$

$$= < 0.5, 0.4 > \{< 0.5, 0.5 > + < 0.0, 1.0 >\} + < 0.2, 0.7 > \{< 0.5, 0.5 > + < 0.2, 0.5 >\}$$

$$+ < 0.1, 0.7 > \{< 0.0, 1.0 > + < 0.8, 0.2 >\}$$
$$= < 0.5, 0.4 >< 0.5, 0.5 > + < 0.2, 0.7 >< 0.5, 0.5 > + < 0.1, 0.7 >< 0.8, 0.2 >$$
$$= < 0.5, 0.5 > + < 0.2, 0.7 > + < 0.1, 0.7 > = < 0.5, 0.5 >$$

SOME PROPERTIES OF IFD

In this section some properties of IFD are presented.

Definition 7 *An IFD is null if all elements of it are zero, i.e., all elements are* $< 0, 0 >$ *and obviously its value is equal to* $< 0, 0 >$.

Definition 8 *An IFD is unit if all diagonal elements are* $< 1, 0 >$ *and all remaining elements are* $< 0, 1 >$ *and it is denoted by* $I_{0,1}$.

The value of a unit IFD is $< 1, 0 >$.

Definition 9 *The transpose* A' *of an IFD* $A = |a_{ij}|_{n \times n}$ *is defined as* $A' = |a_{ji}|_{n \times n}$, *where* $a_{ji} = < a_{ji\mu}, a_{j\nu} >$.

Definition 10 *An IFD* $A = |a_{ij}|_{n \times n}$ *is triangular if either* $a_{ij} = <0, 1>$ *for all* $i > j$ *or* $a_{ij} = < 0, 1 >$ *for all* $i < j$; $i, j = 1, 2, ..., n$.

Theorem 2 *Let A be an IFD of order* $n \times n$. *If all elements of a row (or column) are* $< 0, 1>$ *then its value is equal to* $< 0, 1 >$.

This result is illustrated in Example 3.

EXAMPLE 3 : Let

$$A = \begin{bmatrix} < 0.0, 1.0 > & < 0.0, 1.0 > & < 0.0, 1.0 > \\ < 0.2, 0.5 > & < 0.3, 0.7 > & < 0.8, 0.1 > \\ < 0.7, 0.2 > & < 0.1, 0.2 > & < 0.3, 0.6 > \end{bmatrix}$$

be an IFM. Note that all elements of first row are $< 0, 1 >$.

Now

$$|A| = < 0.0, 1.0 > \begin{vmatrix} < 0.3, 0.7 > & < 0.8, 0.1 > \\ < 0.1, 0.2 > & < 0.3, 0.6 > \end{vmatrix} + < 0.0, 1.0 > \begin{vmatrix} < 0.2, 0.5 > & < 0.8, 0.1 > \\ < 0.7, 0.2 > & < 0.3, 0.6 > \end{vmatrix}$$

$$+ < 0.0, 1.0 > \begin{vmatrix} < 0.2, 0.5 > & < 0.3, 0.7 > \\ < 0.7, 0.2 > & < 0.1, 0.2 > \end{vmatrix}$$

$= < 0.0, 1.0 > \{< 0.3, 0.7 > + < 0.1, 0.2 >\} + < 0.0, 1.0 > \{< 0.2, 0.6 > + < 0.7, 0.2 >\}$
$+ < 0.0, 1.0 > \{< 0.1, 0.5 > + < 0.3, 0.7 >\}$
$= < 0.0, 1.0 >< 0.3, 0.2 > + < 0.0, 1.0 > < 0.7, 0.2 > + < 0.0, 1.0 > < 0.3, 0.5 >$
$= < 0.0, 1.0 > + < 0.0, 1.0 > + < 0.0, 1.0 > = < 0.0, 1.0 >$

Therefore, $|A| = < 0, 1 >$.

Thorem 3 *(i) If A be an IFM then* $|A| = |A^t|$.
(ii) If any two rows (or columns) of an IFD are interchanged then the values remain unchanged.

Theorem 4 *If A is a triangular IFM then*

$$|A| = \prod_{i=1}^{n} a_{ii} = \prod_{i=1}^{n} < a_{ii\mu}, a_{ii\nu} >$$

EXAMPLE 4 : Let

$$A = \begin{bmatrix} < 0.2, 0.1 > & < 0.3, 0.7 > & < 0.3, 0.7 > \\ < 0.0, 1,0 > & < 0.4, 0.5 > & < 0.8, 0.1 > \\ < 0.0, 1.0 > & < 0.0, 1.0 > & < 0.5, 0.5 > \end{bmatrix}$$

be a triangular IFM.

Then

$$|A| = < 0.2, 0.1 > \begin{vmatrix} < 0.4, 0.5 > & < 0.8, 0.1 > \\ < 0.0, 1.0 > & < 0.5, 0.5 > \end{vmatrix} + < 0.3, 0.7 > \begin{vmatrix} < 0.0, 1.0 > & < 0.8, 0.1 > \\ < 0.0, 1.0 > & < 0.5, 0.5 > \end{vmatrix}$$

$$+ < 0.3, 0.7 > \begin{vmatrix} < 0.0, 1.0 > & < 0.4, 0.5 > \\ < 0.0, 1.0 > & < 0.0, 1.0 > \end{vmatrix}$$

$= < 0.2, 0.1 > \{< 0.4, 0.5 > < 0.5, 0.5 > + < 0.0, 1.0 >\}$
$+ < 0.3, 0.7 >< 0.0, 1.0 > + < 0.3, 0.7 >< 0.0, 1.0 > = < 0.2, 0.1 >< 0.4, 0.5 >< 0.5, 0.5 >$
$+ < 0.0, 1.0 > + <0.0, 1.0 >$
$= < 0.2, 0.1 >< 0.4, 0.5 >< 0.5, 0.5 > + < 0.0, 1.0 >$
$= < 0.2, 0.1 >< 0.4, 0.5 >< 0.5, 0.5 >$

which is the product of diagonal elements of A and the final value of $|A|$ is $< 0.2, 0.5 >$.

Let a_{ij} be a member of $< F >$. If a_{ij} is multiplied by a scalar k, $0 \leq k \leq 1$, then membership and non-membership values of a_{ij} are respectively, $ka_{ij\mu}$ and $ka_{ij\nu}$, i.e., $ka_{ij} = < ka_{ij\mu}, ka_{ij\nu} >$.

Theorem 5 *Let B be an IFM obtained from another IFM A by multiplying a scalar k, $0 \leq k \leq 1$, then $|B| = k|A|$.*

Proof. Let $A = [a_{ij}]_{n\times n} = [< a_{ij\mu}, a_{ijv} >]_{n\times n}$. Then $B = [b_{ij}]_{n\times n} = [< ka_{ij\mu}, ka_{ijv} >]_{n\times n}$.
Now,

$$|B| = \sum_{\sigma\in S_n}\prod_{i=1}^{n} b_{i\sigma(i)} = \sum_{\sigma\in S_n}\prod_{i=1}^{n} ka_{i\sigma(i)} = k\sum_{\sigma\in S_n}\prod_{i=1}^{n} a_{i\sigma(i)} = k|A|.$$

Hence the result.

Definition 11 *An IFD $A = |a_{ij}|$ is constant if $a_{ik} = a_{jk}$ for all i, j, k, i.e., all the rows are identical.*

EXAMPLE 5 : Let

$$A = \begin{vmatrix} <0.1, 0.2> & <0.4, 0.7> & <0.5, 0.5> \\ <0.1, 0.2> & <0.4, 0.7> & <0.5, 0.5> \\ <0.1, 0.2> & <0.4, 0.7> & <0.5, 0.5> \end{vmatrix}$$

be a constant IFD.

Then

$$A = <0.1, 0.2>\begin{vmatrix} <0.4, 0.7> & <0.5, 0.5> \\ <0.4, 0.7> & <0.5, 0.5> \end{vmatrix} + <0.4, 0.7>\begin{vmatrix} <0.1, 0.2> & <0.5, 0.5> \\ <0.1, 0.2> & <0.5, 0.5> \end{vmatrix}$$

$$+ <0.5, 0.5>\begin{vmatrix} <0.1, 0.2> & <0.4, 0.7> \\ <0.1, 0.2> & <0.4, 0.7> \end{vmatrix}$$

$$= <0.1, 0.2><0.4, 0.7> + <0.4, 0.7><0.1, 0.5> + <0.5, 0.5><0.1, 0.7>$$
$$= <0.1, 0.7> + <0.1, 0.7> + <0.1, 0.7> = <0.1, 0.7>$$

Note that 0.1 is the least value among the membership values and 0.7 is the greatest value among the non-membership values.

In general we conclude the following result.

Theorem 6 *If A is a constant IFD then its value is*

$$< min_j(a_{ij\mu}), max_j(a_{ijv}) >$$

for any i.

REFERENCES

[1] M. Z. Ragab and E. G. Eman, The determinant and adjoint of a square fuzzy matrix, *Fuzzy Sets and Systems*, 61 (1994) 297-307.

[2] J. B. Kim, Determinant theory and Boolean matrices, *Congressus Numerantium*, (1988) 273-276.

[3] J. B. Kim, A. Baartmans and N. S. Sahadin, Determinant theory of fuzzy matrices, *Fuzzy Sets and Systems*, 29 (1998) 349-356.